BiBeam Specimen Design for investigating Stress Corrosion Cracking in Brittle Materials

A Thesis Presented for the

Master of Science

Degree

The University of Tennessee, Knoxville

Sunday Christopher Aduloju

May 2018

Acknowledgements

I would like to thank my advisor, Dr. Timothy Truster, who provided me with the amazing opportunity to work on his research team. Without his support, none of this would have been possible.

I would also like to thank Prof. John Ma and Dr. Mark Denavit for being on my thesis committee and for providing me with their much-appreciated feedback.

I would like to thank Scott Grutzik, Dave Reedy, and John Emery, of Sandia National Laboratories for initiating this project and providing the needed assistance through-out this project.

This project was completed as part of the Nonlinear Mechanics and Dynamics (NOMAD) Institute, co-hosted by Sandia National Laboratories and the University of New Mexico. I would like to thank Fracture Analysis Consultants (Ithaca, NY) for complimentary use of the Franc3D software.

Finally, I would like to thank my wife, parents and friends who have supported and encouraged me throughout my entire career.

Abstract

The existing method for testing and collecting Stress Corrosion data requires application of externally applied load on the specimen in the corrosive media. We propose a new type of specimen consisting of a bi-beam where two materials having slightly different coefficient of thermal expansions are bonded together and cooled to room temperature such that a self-loaded specimen is produced because of the presence of residual stress. This creates a very stable stress field that is ideal for long-term toughness experiments. A finite element model was developed to design such specimens while ensuring that the crack propagates at a steady state across the specimen. The model was first verified against analytical results for a thin film on a substrate. Then, since non-constant stress intensity factor are desirable for recording a spectrum of response, specimen geometries were investigated to determine the best geometry suitable for such experiments. The results obtained were validated by performing a stress corrosion cracking experiment using Schott B/Soda-lime glass bi-beam in water and the numerical data compares well with the experimental data.

Table of Contents

List of Tables

List of Figures

1. Introduction

Much importance is always attached to the reliability of structures both from the design and manufacturing perspectives. This is because the effects of failure in structure ranges from the simple inconveniences to life threatening or death of user. Stress corrosion cracking (SCC) is an important source of structure failure that is getting continuing attention and research are being focused presently to reduce the effect of the damage caused by SCC.

In the early 19th century, many brass cartridges were rendered useless by the cracks resulting from season cracking and thereby affected the military activity of the British forces in India [1]. 17 people were killed and 9 others were injured in March 4, 1965 from gas pipeline explosion at the north of Natchitoches in Louisiana[2]. About 7 homes which were 450 feet away from where the explosion occurred were said to be destroyed. None of these could be compared to the catastrophic collapse of the Silver Bridge connecting Point Pleasant, West Virginia and Gallipolis, Ohio that occur on 15th of December 1967. 46 people travelling on the bridge were killed and two of the victims were not found [3]. Recently, 14 fatalities were recorded from the collapse of a swimming pool in Moscow [4]. All these collapses were caused by SCC.

For a material placed in non-chemically reactive environment, crack grows when the stress intensity factor is equal to the fracture toughness. If water is present (as it is in almost all practical environments), water molecules can interact with the material at the crack tip to cause slow crack propagation at lower stresses [5, 6]. Relative humidity and temperature both enhance this phenomenon [7, 8].

Stress corrosion cracking is a type of subcritical crack growth of a crack front which occurs when the environmental corrosive agents attack the crack front thereby causing the crack that would otherwise be stable to grow to a point where it becomes critical. As such, SCC is an important factor in determining service life or shelf life of a component.

In the past, SCC has been studied under a variety of conditions but specimens have always

required a load to be externally applied [7-15]. The most common setup requires a double cantilever beam specimen subjected to a constant external loading or bending moment were crack extension are measured as a function of time using optical equipment.

1.1. Gilman-Wiederdon Experiment

This is the most common method for testing and collecting SCC data. Cracks were created using the method already described by Gilman [8, 9, 16, 17] where cutting scratches are usually made on the specimen with a glass cutter and the specimen heated in dry oven and chilling the cut portion to extend the crack. The cut portion at the surface of the specimen is flash heated by glass flame intermittently to further increase the crack length to the required length. The material is then annealed to provide identical structures of more than one specimen for testing.

Figure 1.1 shows the schematic diagram of the Gilman-Wierderdon experimental setup used to study SCC in glass specimens. Specimens of known compositions are usually provided as microscope slides and crack propagation are restricted to midplane of the specimen. Specimens are mounted in a universal testing machine using hooks which passed through the holes, and crack motion are observed using a microscope attached to cathetometer. A constant applied load is maintained during measurements, and crack velocities that range from 10^{-10} to 10^{-2} m/s can be collected through this method [8, 9] .

These measurements are usually collected in a corrosive medium with controlled temperature and data are presented as log of crack velocity versus the stress intensity factor according to
Figure 1.2 shows that three main regions are usually identified in the SCC plots. The region 0 also known as the threshold limit region may sometimes be absent for some materials [18]. The regions associated with SCC have been given brief descriptions in Table 1.1.The classification was based on the ability of the chemical reactant to control crack rate in the specimen. See [8, 9, 18, 19] for more details.

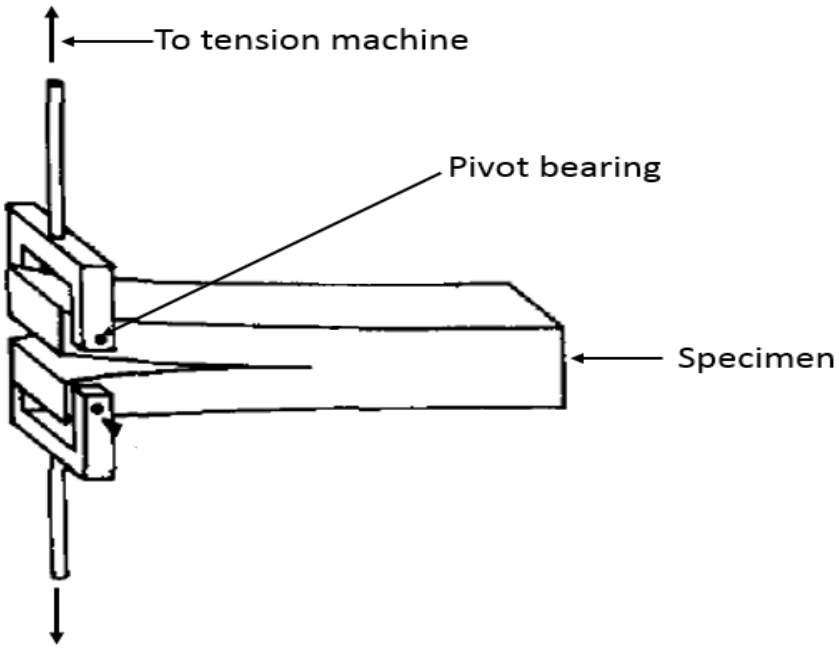

Figure 1.1. Experimental setup

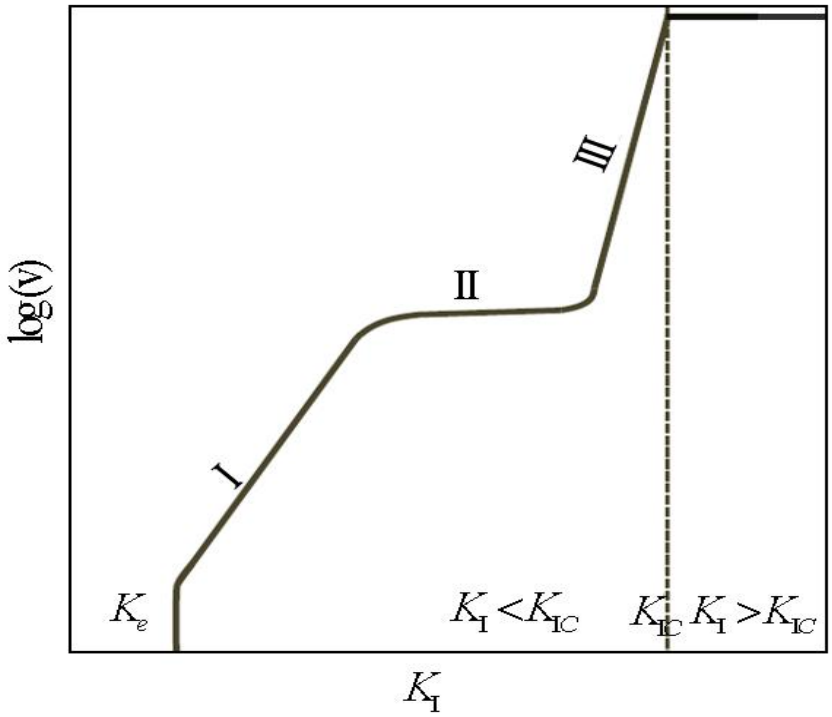

Figure 1.2. The regions of subcritical crack growth associated with stress corrosion cracking [8, 9, 18, 19].

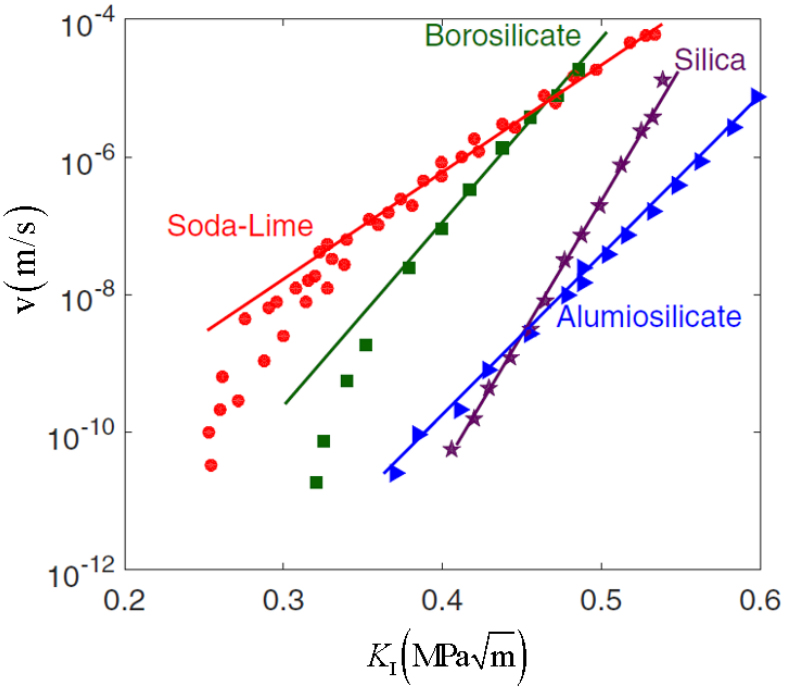

Figure 1.3. Stress corrosion cracking in region 0-I

Table 1.1. The regions of subcritical crack growth associated with stress corrosion cracking.

Region	Description
Region 0	The stresses are too low to cause crack front to move. This region is also known as threshold limit $\left(K_{\mathrm{e}}\right)$
Region I	The velocity of the crack front is controlled by the chemical rate at the crack tip
Region II	The velocity of the crack front is controlled by the time for the chemical reactant to reach the crack front
Region III	The velocity of the crack front is not controlled by the chemical reactant as result of the higher velocity

1.2. Proposed Method

Even with simple dead loading, it can be difficult to guarantee that the load will remain constant over a test that could last months or years [20]. We propose a new type of specimen in Figure 1.4 consisting of a bimaterial beam where the two materials have slightly different coefficient of thermal expansions (CTEs) to study SCC. If both materials are glass, they can be diffusion bonded at a temperature of around 400-600°C. As they cool to room temperature the two materials will contract by different amounts according to their CTE values. Because they are constrained to be the same length along the interface, this puts the composite beam in bending with tensile stresses in the material with the smaller CTE value. Fig. 1 shows the schematic description of the entire bonding process. In this way, the specimen is "self-loaded" by the residual stress resulting from the bonding process. This creates a very stable stress field that is ideal for long-term toughness experiments.

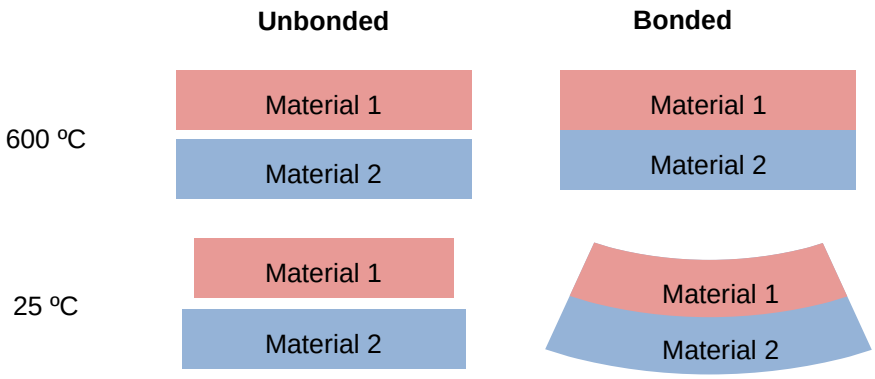

Figure 1.4. Schematic of unbonded and bonded materials cooling from 600°C to 20°C with CTE values CTE_1 and CTE_2 where $CTE_1 > CTE_2$

The objective of this research is to design such a specimen. The bonding temperature and the size of each side of the bibeam need to be picked to provide SIFs between approximately $0.5\,K_{IC}$ and $0.9\,K_{IC}$ where K_{IC} is the fracture toughness of the material in tension under pure Mode I

(tensile) crack opening. The goal is to have SIFs low enough to be sub-critical (less than K_{IC}) but still high enough for propagation to occur in a reasonable amount of time. An important factor to consider is to make sure that once a crack starts to propagate the propagation is stable. Suo and Hutchinson [21, 22] have shown that in this geometry a crack will propagate in the material with smaller CTE and parallel to the interface along a path where $K_{II} = 0$.

Though we present preliminary experimental data to validate the specimen design, this work will be limited to the design of the bibeam specimen. There are ongoing research efforts at the Sandia National Laboratories to develop standardized experimental procedure for this method.

The major sections of this thesis are as follows. The analyses of steady state cracking growth in film-substrate system using analytical and Finite Element (FE) methods are summarized in Chapter 2. The extension of the analyses to steady state cracking growth in rectangular bibeam model are provided in Chapter 3. The design and optimization of bibeam specimen for studying SCC are discussed in Chapter 4. First, the design for SCC in rectangular Scott B/Soda lime glass bibeam is presented in Section 4.1 followed by specimen geometry optimization in Section 4.2 to produce crack growth with non-constant stress intensity factors. The results of the analyses are validated with experimental results in Section 4.3 and conclusions are drawn in Chapter 5.

2. Steady State Crack (SSC) Growth in Film-Substrate Systems

Several attempts have been made to understand the cracking process in film- substrates system. Evans et al [23] shows that several decohesion mechanisms occur for film-substrate systems under the influence of some residual stresses. These mechanisms depend on residual stress type, ductility of the member system, and the quality of the interface bonding. The decohesion mechanisms are summarized in Table 2.1. Early studies [23, 24] have revealed that for films under residual tension, there could be either initial debonding at the edges or formation of the internal crack in the film that would propagate along the interface. The crack growth along the interface for brittle film/brittle substrate system has been shown by experiments [25-27] to deviate into the substrate and propagate steadily parallel to the interface as shown in Figure 2.1 if the substrate fracture toughness is very low.

The observed crack depth was compared with theoretical predictions [22, 27], and it was found out that crack grows at a steady state parallel to the interface when the Mode II stress intensity Factor $K_{II}=0$.

Here-in, we describe the analytical model developed by Suo and Hutchinson [21, 22, 28, 29] for predicting SSC depth in film-substrate systems. First, we define the system geometry. The expression for relative SSC depth λ expressed as the ratio of the of crack depth to thickness of the film or top material is shown in equation (2.1) and the thickness ratio τ can be expressed as the ratio of the thickness of substrate to film in Equation (2.2), where d represents the cracking depth, h is the thickness and subscript 1 and 2 refer to the film and the substrate according to Figure 2.2.

$$\lambda = \frac{d}{h_1} \tag{2.1}$$

$$\tau = \frac{h_2}{h_1} \tag{2.2}$$

Table 2.1. Decohesion mechanism(s) in film/substrate systems

Residual stress	Film/substrate system	Interface bonding	Decohesion mechanism(s)
Tensile	Brittle/ductile	Good	Film cracking: No decohesion
		Poor	Film cracking/Inteface decohesion
	Ductile/brittle	Good	Edge decohesion in substrate
		Poor	Edge decohesion at interface
	Ductile/ductile	Poor	Edge decohesion at interface
		Good	Film/substrate splitting/substrate decohesion
	Brittle/brittle	poor	Edge decohesion at interface, interface cracking/interface decohesion
		Good	Buckle propagation in film
Compressive	Brittle/ductile	Poor	Buckle propagation at interface
		Good	Substrate splitting
	Ductile/brittle	Poor	Buckle propagation at interface
	Ductile/ductile	Good	No decohesion
		Poor	Buckle propagation at interface
	Brittle/brittle	Poor	Buckle propagation at interface

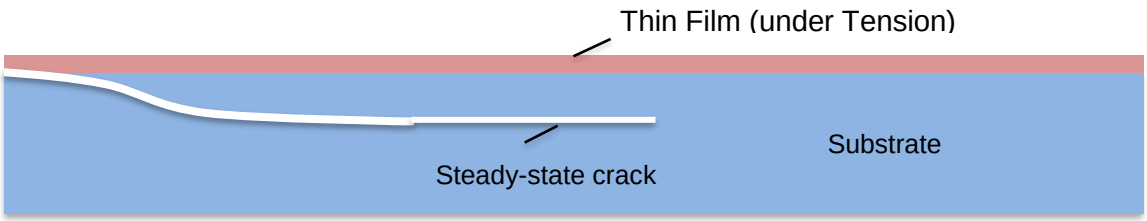

Figure 2.1. Crack propagation in a system consisting of thin film deposited on a substrate

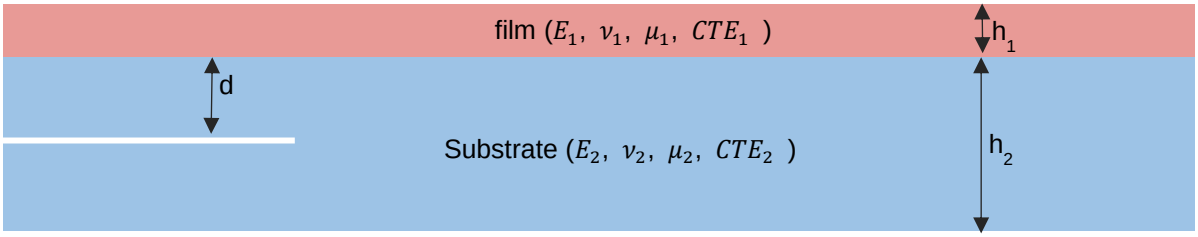

Figure 2.2. film substrate geometry

2.1. Dundurs' Parameter

The understanding of the elastic mismatch between the two materials is very significant in providing accurate modeling of SSC. The elastic mismatch of the two materials could be expressed in terms of two Dundurs' parameters α and β. The parameters are expressed in equation (2.3) and equation (2.4)

$$\alpha = \frac{\Gamma(\kappa_2+1)-(\kappa_1+1)}{\Gamma(\kappa_2+1)+(\kappa_1+1)} \tag{2.3}$$

$$\beta = \frac{\Gamma(\kappa_2-1)-(\kappa_1-1)}{\Gamma(\kappa_2+1)+(\kappa_1+1)} \tag{2.4}$$

where $\Gamma = \mu_1/\mu_2$, $\kappa = 3-4\nu$ for plane strain and $\kappa = (3-\nu)/(1+\nu)$ for plane stress, μ is the shear modulus and ν is the Poisson's ratio. It has been shown that there exists a linear relationship between α and β [6] but the effect of second Dundurs' parameter β is mostly significant for problems involving oscillation at interfacial crack tip, and cracking parallel to the interface is only weakly dependent on β [22, 29, 30]. In this work, we focus on the effect of α.

The First Dundurs' parameter α is the measure of the difference in the stiffness of the upper material to the bottom material of the bimateral beam. $\alpha > 0$ when the top material is stiffer than bottom material of bimaterial beam and $\alpha < 0$ when the top material is more compliant than the bottom material. The sign of α is reversed when material 1 and material 2 are interchanged. The

α parameter can be seen to be between -1 and 1 by letting one of the shear moduli go to zero [31].It has been shown that α parameter can easily be simplified by expressing it in terms of Elastic moduli of the two materials that makes up the bonded material [32]. The simplified form of α is expressed in Equation (2.5).

$$\alpha = \frac{E_2^+ - E_1^+}{E_2^+ + E_1^+} \tag{2.5}$$

Where the expression for E_i^+ is given in Eqn (6).

$$E_i^+ = \begin{cases} \dfrac{E_i}{(1-\nu_i^2)} & (\text{plane strain}) \\ E_i & (\text{plane stress}) \end{cases} \tag{2.6}$$

E_i, ν_i (for i=1,2) represent the elastic moduli and Poisson's ratios of the material components of the bonded material. The stiffness ratio Σ then could be expressed in terms of α in equation

$$\Sigma = \frac{1+\alpha}{1-\alpha} \tag{2.7}$$

2.2. SSC Depth

An attempt has been made to quantify the internal force and moment in the film-substrate system because of the residual stress. Here-in, we summarize the analytical approach for calculating the SCC depth in a substrate beneath thin films.

Figure 2.3 shows a model of film/substrate system without crack while Figure 2.4 shows the cracked model. The equilibrium equation of forces and moments for the cracked model is expressed in (2.8)-(2.9). Both models could be superposed to obtain the simplified model of the problem in Figure 2.5 where the controlling load parameters could be reduced to P and M in (2.10). The reduced force P and moment M resulting from the residual tensile stress σ of the film is expressed through the solutions in (2.11)-(2.12). See [22] for details.

Figure 2.3. The model of film/substrate system without crack

Figure 2.4. The model of film/substrate system with crack

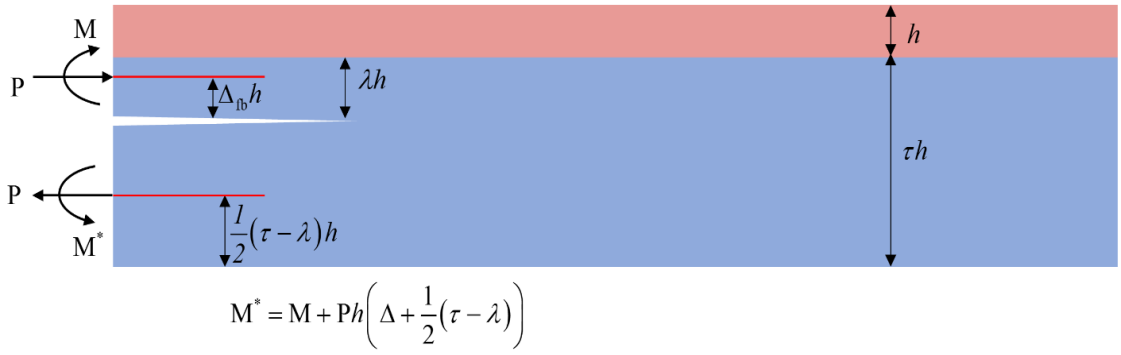

Figure 2.5. The superposed model

$$P_1 + P_2 - P_3 = 0 \tag{2.8}$$

$$M_2 + M_1 - M_3 - P_3 h\left(\Delta_{fb} + \tau/2 - \lambda/2\right) + P_1 h\left(\Delta_{fb} - \tau/2 + \lambda/2\right) = 0 \tag{2.9}$$

$$P = P_3 - C_1 P_1 - C_2 M_1/h, \quad M = M_3 - C_1 M_1 \tag{2.10}$$

$$P = \sigma h_1 \left[1 - C_1 - C_2\left(0.5 + \tau - \Delta_{fa}\right)\right] \tag{2.11}$$

$$M = \sigma h_1^2 \left[\left(0.5 + \lambda - \Delta_{fb}\right) - C_3\left(0.5 + \tau - \Delta_{fa}\right)\right] \tag{2.12}$$

$$C_1 = \frac{A_{fb}}{A_{fa}},\ C_2 = \frac{A_{fb}}{I_{fa}}\left[\left(\tau - \Delta_{fa}\right) - \left(\lambda - \Delta_{fb}\right)\right],\ C_3 = \frac{I_{fb}}{I_{fa}} \tag{2.13}$$

Where σ is the misfit or residual stress in the film, Δ, A, I are the position of the neutral axis, dimensionless effective cross-sectional area, and moment of inertia of the beam per unit width obtained from the upper beam far behind the crack tip fb and the layers far ahead of the crack tip fa. Therefore Δ_{fa}, A_{fa} and I_{fa} are obtained from the composite beam section consisting of film and substrate, and Δ_{fb}, A_{fb} and I_{fb} are obtained from the composite beam section consisting of film and spalled portion of the substrate. Recall that λ and τ are already expressed in (2.1) and (2.2).

$$A_{fb} = \lambda + \Sigma, \quad A_{fa} = \tau + \Sigma \tag{2.14}$$

$$I_{fb} = \left\{\Sigma\left[3\left(\Delta_{fb} - \lambda\right)^2 - 3\left(\Delta_{fb} - \lambda\right) + 1\right] + 3\Delta_{fb}\lambda\left(\Delta_{fb} - \lambda\right) + \lambda^3\right\} \tag{2.15}$$

$$I_{fa} = \left\{\Sigma\left[3\left(\Delta_{fa} - \tau\right)^2 - 3\left(\Delta_{fa} - \tau\right) + 1\right] + 3\Delta_{fa}\tau\left(\Delta_{fa} - \tau\right) + \tau^3\right\}$$

$$\Delta_{fa} = \frac{\tau^2 + 2\Sigma\tau + \Sigma}{2\left(\tau + \Sigma\right)} \tag{2.16}$$

$$\Delta_{fb} = \frac{\lambda^2 + 2\Sigma\lambda + \Sigma}{2\left(\lambda + \Sigma\right)}$$

$$\sigma = \frac{E_1 \left(CTE_1 - CTE_2\right)\left(T_d - T_r\right)}{\left(1-\upsilon_1\right)} \tag{2.17}$$

The misfit stress is found to be a function of the film poisson ratio υ_1, difference between the coefficient of thermal expansions $CTEs$, and the temperature difference between the film deposition temperature T_d and room temperature T_r. The stress intensity factors have been found to be linearly dependent on the reduced load P and moment M [22, 29]. The mode I stress intensity factor and mode II stress intensity factor could be expressed as

$$K_I = \frac{P}{\sqrt{2Uh_1}}\cos\omega + \frac{M}{\sqrt{2Vh_1^3}}\sin\left(\omega+\gamma\right) \tag{2.18}$$

$$K_{II} = \frac{P}{\sqrt{2Uh_1}}\sin\omega - \frac{M}{\sqrt{2Vh_1^3}}\cos\left(\omega+\gamma\right) \tag{2.19}$$

where U and V are dimensionless positive numbers expressed as

$$U = \frac{A_{fb}\left(\tau-\lambda\right)^3}{\left(\tau-\lambda\right)^3 + A_{fb}\left(\tau-\lambda\right)^2 + 12A_{fb}\left[\Delta_{fb} + \frac{\left(\tau-\lambda\right)}{2}\right]^2} \tag{2.20}$$

$$V = \frac{I_{fb}\left(\tau-\lambda\right)^3}{\left(\tau-\lambda\right)^3 + 12I_{fb}} \tag{2.21}$$

$$\gamma = \sin^{-1}\left\{\frac{12\sqrt{UV}\left[\Delta_{fb} + \left(\tau-\lambda\right)/2\right]}{\left(\tau-\lambda\right)^3}\right\} \tag{2.22}$$

The angle ω is usually obtained from tables and it is independent on α, β, τ and λ. However, the tables prepared for the $\tau = \infty$ and $\tau = 10$ in Table 2.2-Table 2.5 show that ω weakly depends on β and for this reason, the subsequent Table 2.6 and Table 2.7 were presented with β set to zero. It has been shown that for materials with the same or very close elastic mismatch $\alpha = 0$, the value of ω is not affected by the value of λ and $\omega = 52.14^0$ is usually used [27]

and the value of $\omega = 52^0$ could be used as a good approximation for all other values of λ [21, 22].

The steady state cracking depth is obtained when $K_{II} = 0$. The strict enforcement of this condition on equation (2.19) provides the consistent condition of equation (2.23) that must be true for steady state cracking in film-substrate systems. Therefore, the crack depth is truly a steady state cracking depth λ when equation (2.23) is satisfied. We note here that previous discussions only consider the initial crack in the substrate.

$$\frac{\cos(\omega+\gamma)}{\sin\omega} - \sqrt{\frac{V}{U}}\frac{Ph_1}{M} = 0 \tag{2.23}$$

Table 2.2. The angle ω (in degrees) for $\tau = \infty$ and α ranging from -0.8 to 0 [22]

α	-0.8		-0.6		-0.4		-0.2		0.0	
λ β	-0.4	0.0	-0.4	0.0	-0.3	0.1	-0.3	0.1	-0.2	0.2
0.1	45.7	44.3	46.4	45.4	47.6	47.5	49.7	49.8	51.8	53.1
0.5	54.9	52.4	55.6	52.0	54.7	51.1	55.1	51.0	54.2	50.5
1	54.4	53.1	55.2	53.2	54.7	52.5	54.6	51.9	53.5	50.8
1.5	53.5	52.9	54.2	53.1	54.1	52.7	53.9	52.2	53.0	51.2
2	53.1	52.7	53.6	52.9	53.5	52.6	53.4	52.3	52.7	51.4
3	52.6	52.4	52.8	52.5	52.9	52.5	52.8	52.3	52.4	51.7
4	52.3	52.4	52.5	52.4	52.6	52.4	52.5	52.2	52.2	51.8
5	52.3	52.2	52.4	52.3	52.5	52.3	52.4	52.3	52.2	52.0
6	52.2	52.1	52.3	52.3	52.4	52.3	52.3	52.2	52.2	52.0
10	52.1	52.1	52.1	52.1	52.1	52.1	52.1	52.1	52.0	52.0

Table 2.3. The angle ω (in degrees) for $\tau = \infty$ and α ranging from 0 to 0.8 [22]

α	0.0		0.2		0.4		0.6		0.8	
λ β	-0.2	0.2	-0.2	0.2	-0.1	0.3	-0.1	0.3	0.0	0.4
0.1	51.8	53.1	54.6	56.4	58.0	61.3	61.9	66.0	68.5	75.3
0.5	54.2	50.5	54.9	51.0	54.8	51.4	56.9	53.5	60.3	58.0
1	53.5	50.8	53.2	50.1	52.2	49.2	52.5	49.1	53.3	50.0
1.5	53.0	51.2	52.4	50.3	51.2	48.9	50.5	47.8	49.7	46.8
2	52.7	51.4	52.1	50.5	50.8	49.1	49.6	47.6	47.8	45.5
3	52.4	51.7	51.7	50.9	50.6	49.7	49.1	47.9	46.4	44.9
4	52.2	51.8	51.7	51.2	50.6	50.0	49.2	48.4	46.2	45.1
5	52.2	52.0	51.8	51.5	50.9	50.5	49.4	48.9	46.4	45.6
6	52.2	52.0	51.8	51.6	51.0	50.8	49.6	49.3	46.7	46.1
10	52.0	52.0	51.8	51.7	51.4	51.3	50.4	50.2	47.9	47.7

Table 2.4. The angle ω (in degrees) for $\tau = 10$ and α ranging from -0.8 to 0 [22]

α	-0.8		-0.6		-0.4		-0.2		0.0	
λ β	-0.4	0.0	-0.4	0.0	-0.3	0.1	-0.3	0.1	-0.2	0.2
0.5	54.8	52.3	55.4	52.0	54.5	51.0	54.7	50.9	53.9	50.4
1	54.0	52.8	54.8	52.9	54.4	52.2	54.3	51.8	53.3	50.7
1.5	53.1	52.5	53.8	52.7	53.6	52.3	53.4	51.9	52.6	50.9
2	52.5	52.2	52.9	52.3	52.8	52.0	52.7	51.7	52.0	50.9
3	51.5	51.4	51.7	51.4	51.6	51.3	51.5	51.0	51.0	50.4
4	50.4	50.3	50.4	50.4	50.4	50.2	50.2	50.0	49.8	49.5
5	49.0	49.0	49.1	49.0	49.0	48.9	48.9	48.7	48.6	48.4

Table 2.5. The angle ω (in degrees) for $\tau = 10$ and α ranging from 0 to 0.8 [22]

α	0.0		0.2		0.4		0.6		0.8	
λ β	-0.2	0.2	-0.2	0.2	-0.1	0.3	-0.1	0.	0.0	0.4
0.5	53.9	50.4	54.5	50.9	54.5	51.4	56.4	53.5	59.4	57.8
1	53.3	50.7	53.0	50.2	52.0	49.2	52.3	49.3	53.1	50.5
1.5	52.6	50.9	52.0	50.1	50.8	48.8	50.3	48.0	49.9	47.6
2	52.0	50.9	51.4	50.1	50.2	48.8	49.2	47.6	48.1	46.4
3	51.0	50.4	50.4	49.7	49.3	48.6	48.2	47.3	46.6	45.6
4	49.8	49.5	49.3	49.0	48.5	48.1	47.4	46.9	45.8	45.2
5	48.6	48.4	48.1	48.0	47.5	47.2	46.6	46.3	45.1	44.8

Table 2.6. The angle ω (in degrees) for $\tau = \infty$, β=0 and α [22]

λ / α	-0.8	-0.6	-0.4	0.2	0	0.2	0.4	0.6	0.8
0.05	39.8	42.4	45.8	48.9	52.0	55.5	59.2	63.6	70.0
0.1	44.3	45.2	47.2	49.5	52.0	55.1	58.4	62.7	68.5
0.2	48.7	48.3	49.3	50.4	52.0	54.2	57.0	60.6	66.3
0.3	50.8	50.2	50.6	51.1	52.0	53.6	55.7	58.7	64.0
0.4	51.8	51.6	51.4	51.5	52.0	53.1	54.6	57.1	61.9
0.5	52.4	52.3	52.0	51.8	52.0	52.7	53.7	55.8	60.1
0.6	52.7	52.7	52.3	52.0	52.0	52.4	53.0	54.6	58.3
0.7	53.1	52.9	52.6	52.2	52.0	52.1	52.5	53.6	56.8
0.8	53.1	53.1	52.8	52.3	52.0	51.9	52.0	52.8	55.5
0.9	53.2	53.2	52.9	52.4	52.0	51.8	51.7	52.1	54.3
1.0	53.1	53.2	52.9	52.5	52.0	51.7	51.4	51.5	53.3
1.2	53.0	53.2	53.0	52.5	52.0	51.5	50.9	50.6	51.5
1.4	52.9	53.1	53.0	52.6	52.0	51.4	50.6	50.0	50.2
1.6	52.8	53.1	52.9	52.6	52.0	51.3	50.5	49.5	49.2
1.8	52.8	53.0	52.8	52.6	52.0	51.3	50.3	49.2	48.4
2.0	52.7	52.9	52.8	52.5	52.0	51.3	50.3	49.0	47.8
3.0	52.4	52.5	52.6	52.4	52.0	51.4	50.3	48.7	46.4
4.0	52.3	52.4	52.4	52.3	52.0	51.4	50.4	48.9	46.2
5.0	52.2	52.3	52.3	52.2	52.0	51.5	50.7	49.2	46.3
6.0	52.1	52.2	52.2	52.2	52.0	51.6	50.9	49.6	46.6
7.0	52.1	52.2	52.2	52.2	52.0	51.7	51.1	49.8	47.0
8.0	52.1	52.1	52.2	52.1	52.0	51.7	51.1	50.1	47.3
9.0	52.1	52.1	52.1	52.1	52.0	51.8	51.2	50.3	47.6
10.0	52.1	52.1	52.1	52.1	52.0	51.8	51.3	50.3	47.9

Table 2.7. The angle ω (in degrees) for $\tau = 10$, β=0 and α [22]

λ / α	-0.8	-0.6	-0.4	0.2	0	0.2	0.4	0.6	0.8
0.05	39.9	42.4	45.6	48.9	52.2	55.5	59.1	63.3	70.0
0.1	44.3	45.0	47.0	49.5	52.2	55.1	58.5	62.4	67.9
0.2	48.8	48.4	49.1	50.4	52.1	54.3	56.9	60.4	65.6
0.3	50.8	50.2	50.4	51.0	52.1	53.5	55.6	58.5	63.3
0.4	51.8	51.3	51.2	51.4	52.0	52.9	54.4	56.8	61.2
0.5	52.3	52.0	51.7	51.7	51.9	52.5	53.5	55.4	59.4
0.6	52.6	52.4	52.1	51.9	51.9	52.1	52.8	54.3	57.8
0.7	52.8	52.6	52.3	52.0	51.9	51.9	52.3	53.4	56.4
0.8	52.8	52.8	52.5	52.2	51.9	51.7	51.8	52.6	55.1
0.9	52.9	52.9	52.6	52.3	41,9	51.6	51.5	51.9	54.1
1.0	52.9	52.9	52.7	52.3	51.9	51.4	51.2	51.4	53.1
1.2	52.8	52.9	52.7	52.3	51.8	51.2	50.7	50.5	51.6
1.4	52.6	52.8	52.6	52.2	51.7	51.2	50.4	49.9	50.4
1.6	52.5	52.6	52.5	52.1	51.6	50.9	50.1	49.4	49.4
1.8	52.3	52.5	52.4	52.0	51.5	50.8	49.9	49.0	48.7
2.0	52.2	52.3	52.0	51.9	51.4	50.7	49.8	48.8	48.1
3.0	51.4	51.4	51.4	51.1	50.7	50.0	49.1	47.9	46.6
4.0	50.4	50.4	50.3	50.0	49.7	49.2	48.4	47.3	45.8
5.0	49.0	49.1	48.9	48.8	48.5	48.0	47.4	46.5	45.1
6.0	47.5	47.5	47.4	47.2	46.8	46.4	45.9	45.4	44.2

2.3.Film Decohesion and Determination of Crack Path Preference

The non-dimensional Ω parameter associated with the steady state cracking depth is presented in equation (2.24). The decohesion number provides the critical combination of stress σ and film thickness below which steady state cracking in the substrate is inhibited if the fracture toughness K_{IC} is known. The variation in the critical cracking number Ω_c for different α parameters is presented in Figure 2.6.

$$\Omega = \frac{K_{\mathrm{I}}}{\sigma\sqrt{h}} \tag{2.24}$$

The strain energy per unit width per unit length stored in the system far behind the crack tip and far ahead of the crack tip are presented in equation (2.25) and (2.26) in terms of the misfit stress, film thickness, elastic mismatch, cross-sectional area and moment of inertia. The stain energy release rate in equation (2.27) is obtained by taking the difference between the strain energies.

$$G_{\mathrm{fb}} = \frac{\sigma^2 h_1 (1+\alpha)}{16}\left[\frac{1}{\mathrm{A}_{\mathrm{fb}}} + \frac{\left(\lambda - \Delta_{\mathrm{fb}} + 0.5\right)^2}{I_{\mathrm{fb}}}\right] \tag{2.25}$$

$$G_{\mathrm{fa}} = \frac{\sigma^2 h_1 (1+\alpha)}{16}\left[\frac{1}{A_{\mathrm{fa}}} + \frac{\left(\tau - \Delta_{\mathrm{fa}} + 0.5\right)^2}{I_{\mathrm{fa}}}\right] \tag{2.26}$$

$$G = \frac{\sigma^2 h_1 (1+\alpha)}{16}\left[\frac{1}{A_{\mathrm{fb}}} + \frac{\left(\lambda - \Delta + 0.5\right)^2}{I_{\mathrm{fb}}} - \frac{1}{A_{\mathrm{fa}}} - \frac{\left(\tau - \Delta_0 + 0.5\right)^2}{I_{\mathrm{fa}}}\right] \tag{2.27}$$

$$\frac{G_{\mathrm{c}}}{G_{\mathrm{ic}}} < \frac{G}{G_{\mathrm{i}}} \tag{2.28}$$

The strain energy release rate at the interface G_i could be calculated from equation (2.27) by simply taking $\lambda = 0$. The likelihood of the crack to grow by substrate cracking is favored more than interface cracking if equation (2.28) is true. In equation (2.28), G_c and G_{ic} represent the

substrate toughness and interface toughness. Energy release ratio for different film substrate systems is shown in Figure 2.7.

2.4.Finite Element Method

The finite element method provides an alternative solution to boundary value problems for partial differential equations. Finite element method subdivides a large problem into simpler finite elements and provides approximate solution to the unknowns at discrete number of points over the whole domain.

2-dimensional (2D) plane stress finite element simulations were performed using FE modeling capabilities of the commercial FEA code ABAQUS [12].

The material properties required for the FE modeling are Elastic moduli, Poisson's ratio, and CTE. The materials' data were obtained from Sandia National Laboratories and from relevant literature. Each of the materials was assumed to be isotropic and linearly elastic and initial crack length of 15mm was assumed to be present in the substrate. Boundary conditions were applied to restrict rigid body modes and displacements were otherwise free. All FE models were discretized using quadratic Quadrilateral (Q8) elements with a mesh focused mesh structure and quadratic quarter point elements at the crack tip. The method of J contour integral was applied to evaluate stress intensity factors.

Analytic model described earlier was used as a benchmark to check the accuracy of the FE model. This was done by comparing the results obtained from studying the SSC in a film-substrate system. For earlier validation of the finite element model, the SSC in brittle substrates beneath adherent films were modeled for α values of -0.8, -0.6, -0.4, -0.2, 0,0.2, 0.4,0.6 and 0.8 and were compared to the analytical results obtained from [7].

The two dimensions of the substrate used were 150mm length by 25.4 mm thick, and the initial crack length of 15mm was used for all models.

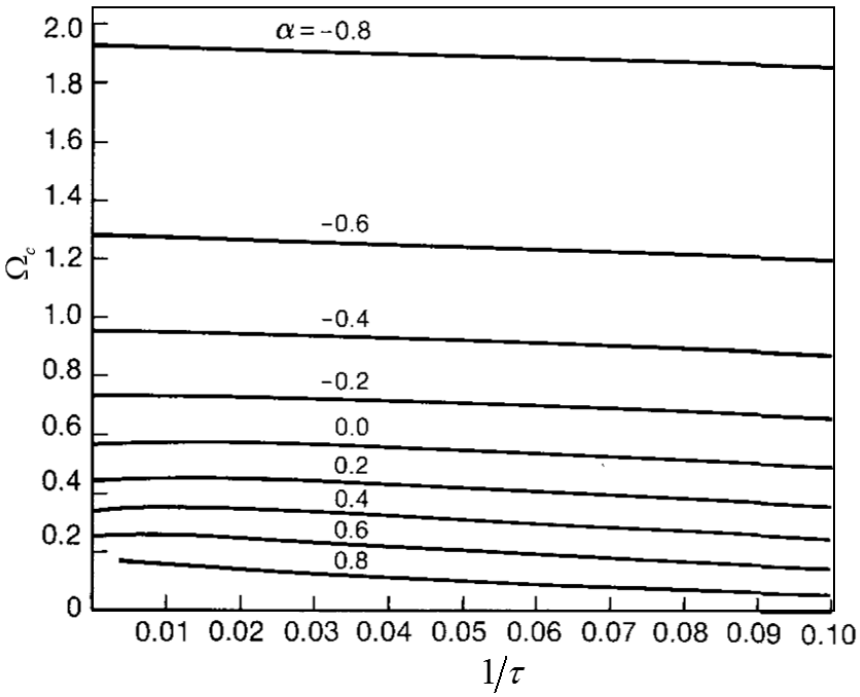

Figure 2.6. The critical cracking number for different film-substrate systems

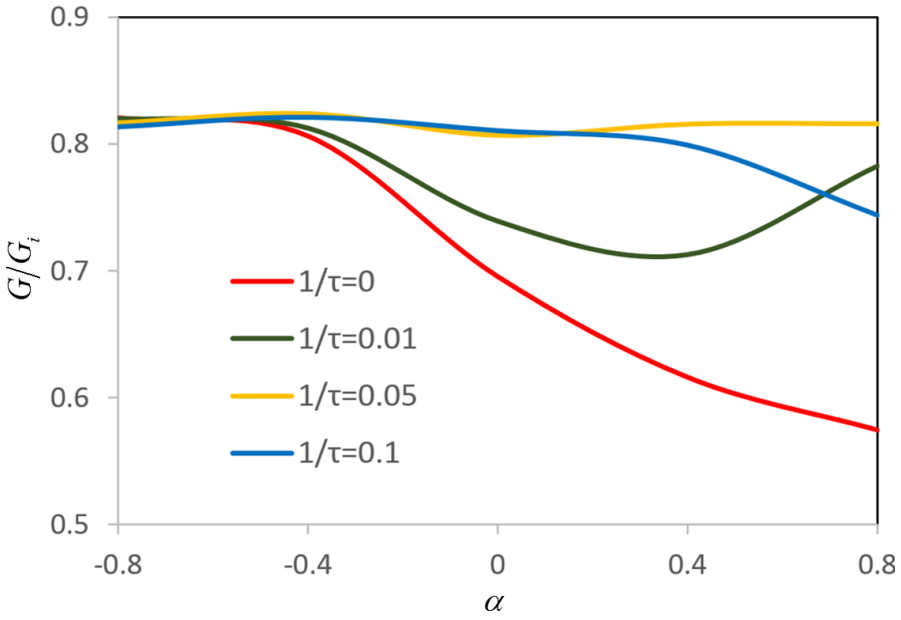

Figure 2.7. Energy release ratio for different film substrate system

The film and the substrate have equal length while the thickness of the film was gradually increased by increasing t $1/\tau$ from 0 up to 0.1. The SSC depth and K_I when K_{II}=0 were determined and the results were compared to the analytical results. h_1 represents the thickness of the film and h_2 the thickness of the glass substrate.

Figure 2.8 shows the stress contour plot with the stress singularity at the crack tip for model having $1/\tau = 0.1$. Figure 2.9 shows the relative SSC depth obtained for different film-substrate thickness ratio $1/\tau$ .These values were obtained for 8 different bonded materials. α_a and α_r represent the choice of first Dundurs' parameter for analytical and FE models. The relative SSC depth decreases with increase in thickness ratio $1/\tau$ and larger crack depth are collected for stiffer films. $1/\tau_a$ and $1/\tau_r$ in Figure 2.10 represent thickness ratio used for analytical and FE model, and the results show that the difference in SSC depth is more for larger α values. The results obtained from the FE model in Figure 2.9 and Figure 2.10 compared well with the results obtained from analytical model.

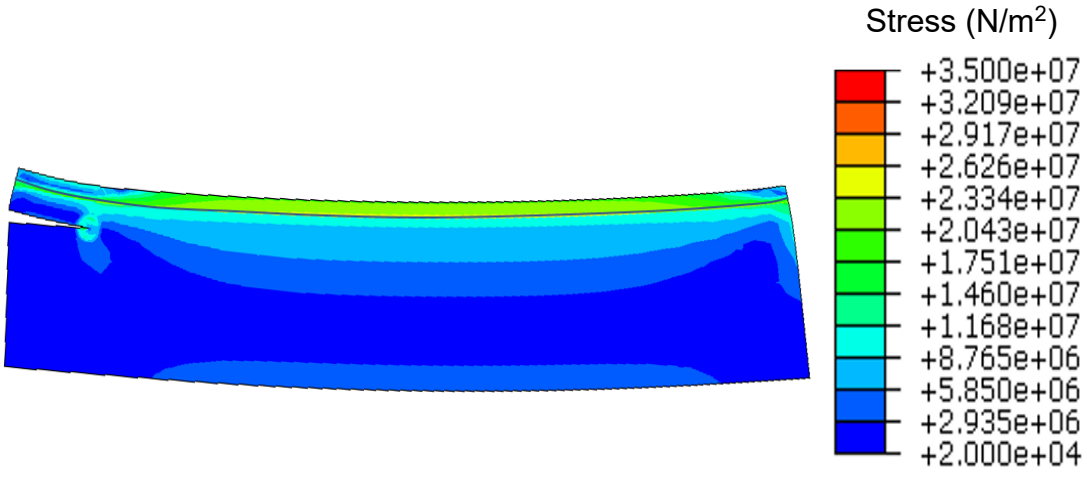

Figure 2.8. The stress contour plot across the film-substrate system

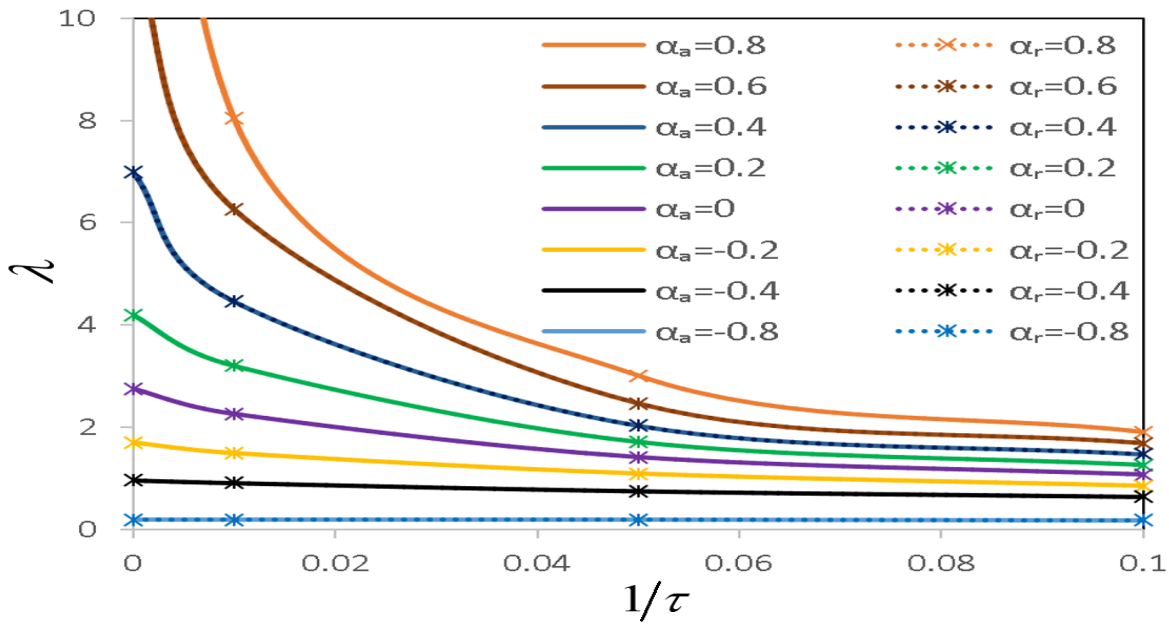

Figure 2.9. Relative SSC depth as function of film/substrate thickness

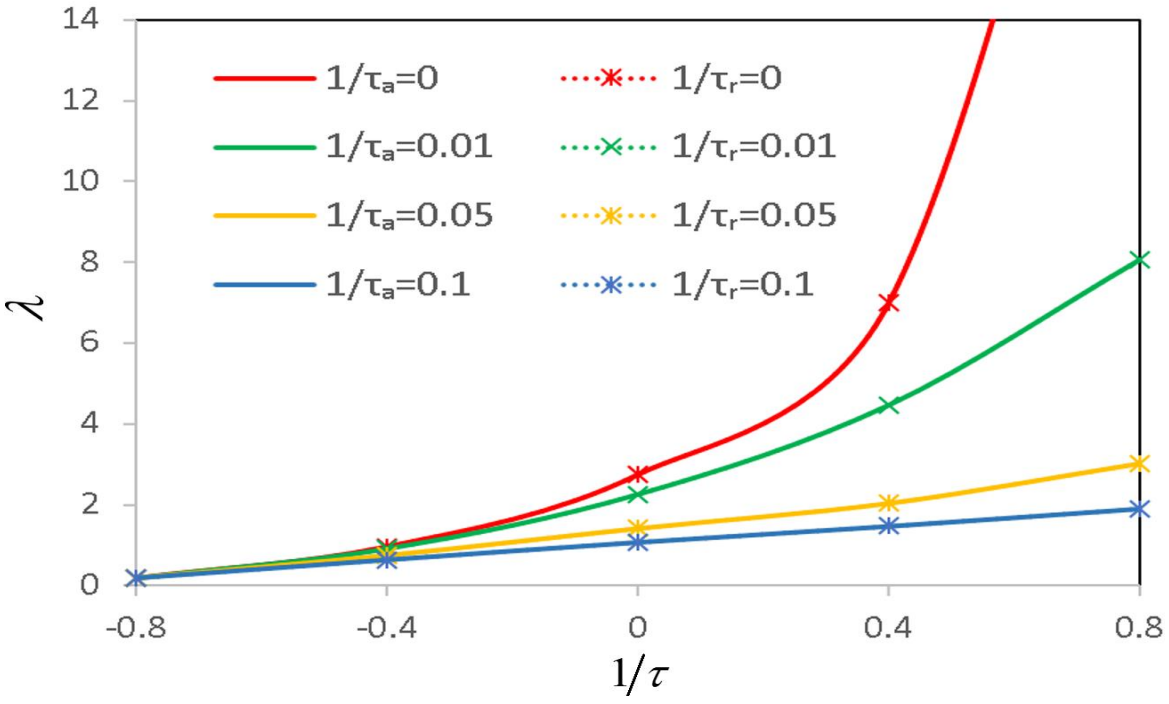

Figure 2.10. Relative SSC depth as a function of Dundurs' parameter, (α)

3. SSC Growth in Bibeam

The analytical model developed for steady state cracking in thin-film substrate were based on consideration of the system as a composite beam. It is only logical to extend the model to prediction of steady state cracking in bibeam in Figure 3.1 where the SSC depth is predicted in the bottom material of bibeam. However, we note the difference between the systems resides primarily in the difference in the limit of the thickness ratio.

1. The top-bottom thickness ratio for film-substrate $1/\tau$ in chapter 2 was shown to be $0<1/\tau\leq 0.1$. Here in, the top-bottom thickness for bibeam is $0.1<1/\tau\leq 10$ but we will restrict $1/\tau$ to $0.1<1/\tau\leq 1$ for most of the analysis performed in this section.
2. The bending moment resulting from the residual stress is larger than those from the thin-film substrate system.

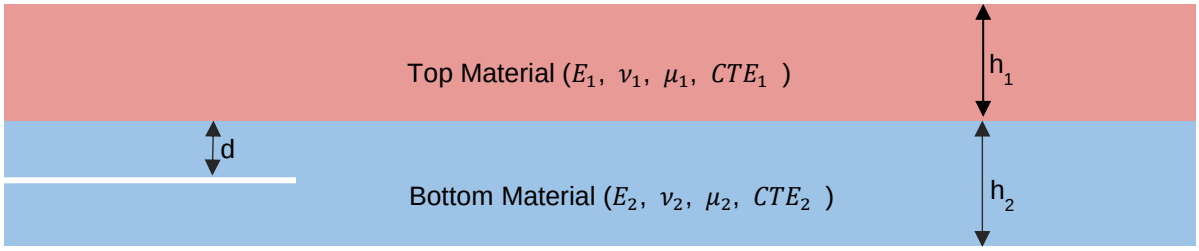

Figure 3.1. Bibeam geometry

Both materials are assumed to be brittle, linear elastic and isotropic. It follows that the earlier model developed in chapter 2 could be used where h_1 and h_2 represent the thickness of the top material and bottom material of the bibeam, and the misfit stress is expressed as (3.1) where T_b is the bonding temperature of the bibeam.

$$\sigma = \frac{E_1 \left(CTE_1 - CTE_2 \right) \left(T_b - T_r \right)}{\left(1 - \upsilon_1 \right)} \tag{3.1}$$

3.1. Methods Comparison for Bibeam

The analytical model and FE model performance for modeling SSC in bibeam are evaluated by extending the methods to study SSC in Soda lime glass. The materials used for this study were Schott B270 (a variant of soda-lime glass) as the top material and standard soda-lime glass as the bottom material. The material properties are shown in Table 3.1. It is important to note $\alpha = 0$ for the bibeam because the elastic moduli of the component are very close. The material components were picked because of the ready availability of the materials. The modeling of the bibeam was accomplished by increasing the thickness ratio $1/\tau$ from 0.1 to 1 while retaining the initial crack length, thickness and length of the bottom material as 15mm, 25.4mm and 150mm. The SSC depth and K_I when $K_{II} = 0$ were determined.

Table 3.1. Material property for the bibeam

Material	Schott B270	Soda-lime
Elastic Modulus (GPa)	71.5	74
Poisson's Ratio	0.22	0.24
CTE (20ºC-600ºC)	1.11185 X 10^{-5}	1.0156 X 10^{-5}

Figure 3.2 shows the stress contour plot across the bibeam with $h_1 = h_2 = 25.4\text{mm}$ and the initial crack length 15mm located at $\lambda = 0.5$. The cooling of the bibeam from the bonding

temperature puts the composite beam in bending because they are constrained to be of the same length along the interface. The bottom material has lower CTE and contracts lesser than the top material. The difference in the contraction of the top material causes bending that produces tensile stresses and compressive stresses at the material interface; however, the maximum stress is produced at the crack tip due to stress singularity.

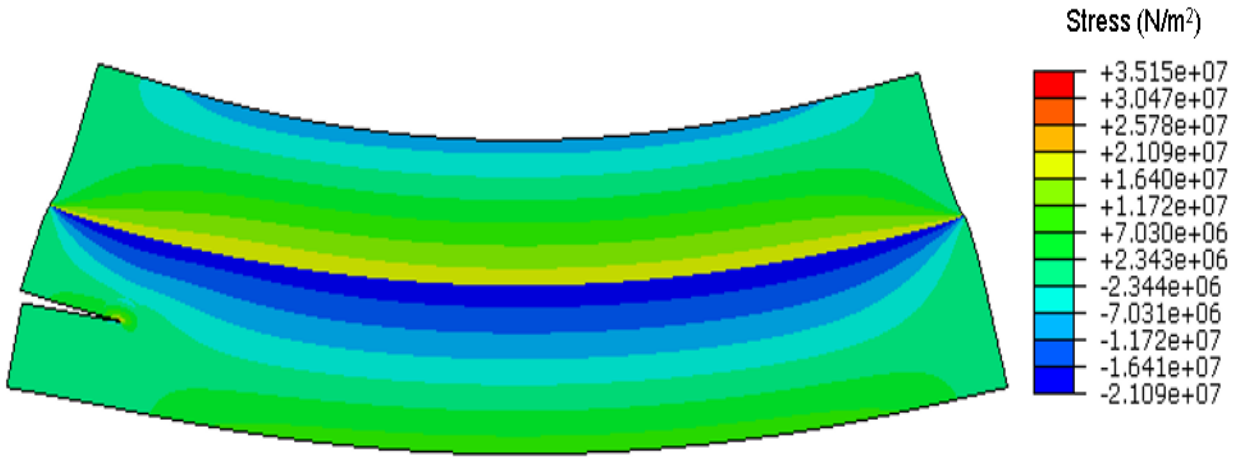

Figure 3.2. The stress (von mises) contour plot across the bibeam

The results obtained from the FE model were compared to the analytical methods and the relative SSC depth obtained from the two models in Figure 3.3 were the same for both thin film-substrate and bibeam models, but the analytical method overestimates the mode I stress intensity factor K_I for the bibeam in Figure 3.4. The analytical model was derived for a thin/film system which is typical for semiconductors application. The thin film assumption used in the analytical model works well for crack propagation in a system with a thin top material because the dominant driving force is mostly tensile stress and the effect from bending is very small. This assumption no

longer holds for the bibeam problem because the driving force for this problem is predominantly bending stresses. Also, a conservative estimate $\omega = 52.^{0}$ described in chapter 2 for thin/substrate system was used for the entire simulation which may no longer hold true for a bibeam specimen.

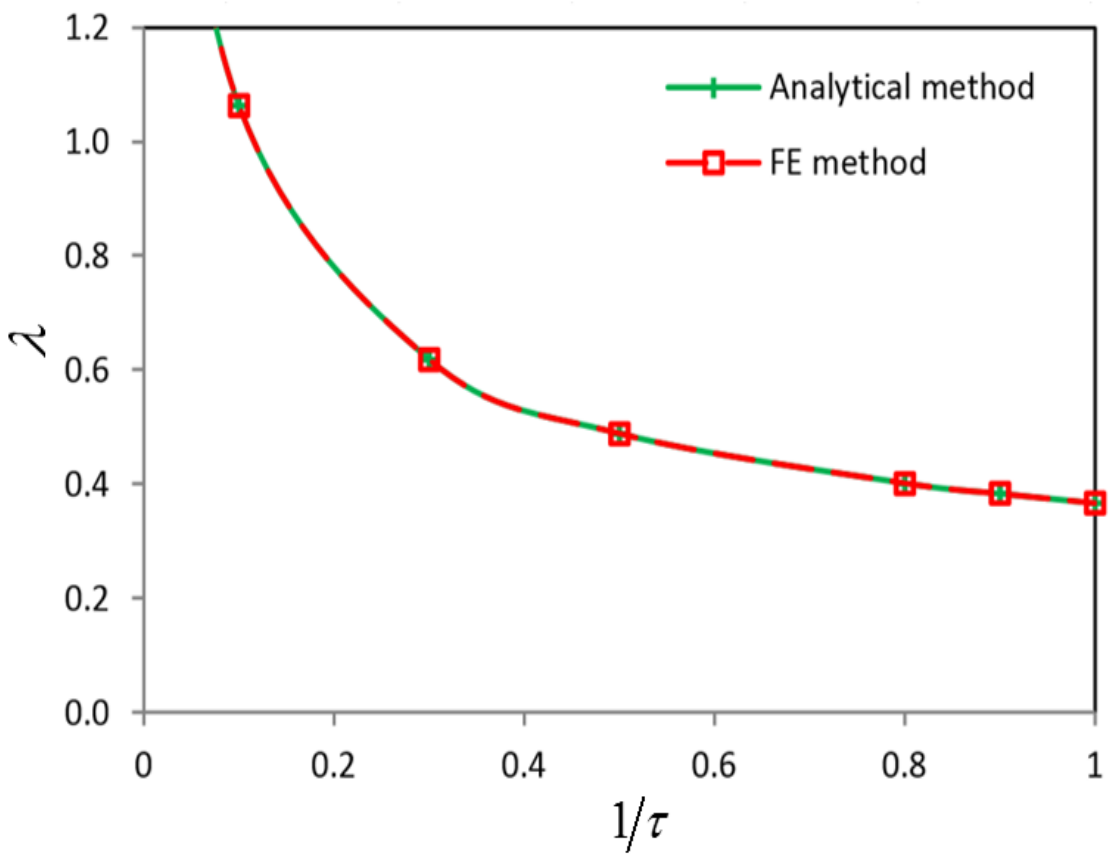

Figure 3.3. Relative cracking depth comparison between the FE and analytical models

3.2. SSC in Rectangular Bibeam Specimen

We have earlier described the SCC depth as the depth in the bottom material where the crack propagates parallel to the interface. We have also shown that this depth could be obtained using the finite element method or analytical method to calculate the depth where $K_{II} = 0$.

Initial FEM simulations were done using Abaqus software and K_I and K_{II} were recorded across

the depth of the bottom material. Though for all simulations we expect the K_{II} to vary across the depth, even variation from negative values to positive values are possible, K_I values can only be positive since we do not want inter-penetrability of the crack faces. Negative values of K_I implies that the stresses ahead of the crack are compressive and square root singular. We provide the SIFs for both mode I and mode II across the bottom material of a rectangular beam in Figure 3.5. The specimen was designed such that the thickness and length of the bottom material remained as 25.4mm and 150mm, respectively, and the top material dimensions were the same as the bottom material. This represents a case study of $1/\tau = 1$.

The initial crack length, thickness and length of the bottom material for this model are 15mm, 25.4mm and 150mm. The K_I when $K_{II} = 0$ are the extracted from this plots for all α. As an example, this study was conducted for three different bibeams having $\alpha = 0.2$, 0 and -0.2. Usually the K_I extracted from Figure 3.5 are used to generate the plot of K_I at SSC depth for all thickness ratio. Therefore, the three K_I values obtained from Figure 3.5 represents three data points at $1/\tau = 1$ in Figure 3.6.The SCC depth were also recorded and plotted in Figure 3.7 for all thickness ratio $0.1 < 1/\tau \leq 0.1$ and results show a steep reduction in the SSC depth that gradually reduces the influence of the $1/\tau$ when $1/\tau > 0.5$.

The results obtained from Figure 3.6 and Figure 3.7 show that the bibeam with residual stresses could be used as specimens for studying SCC since the requirement of straight cracks growth in the specimen could be realized and the necessary requirements for specimen design for SCC could easily be obtained from the plots. The specimen geometry and the location of the initial crack based on the required initial K_I are the outputs from this endeavor. FEM has proven to be a very good tool for realizing the above objectives.

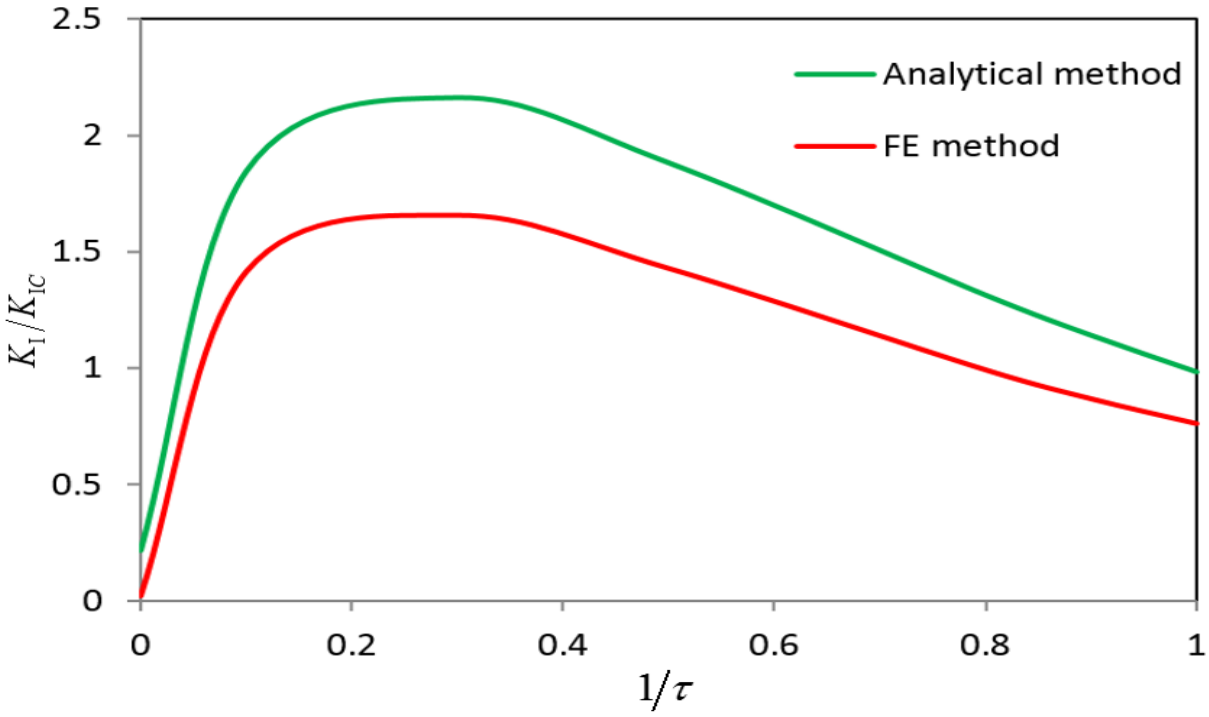

Figure 3.4. K_I at SSC depth obtained from FE and analytical models

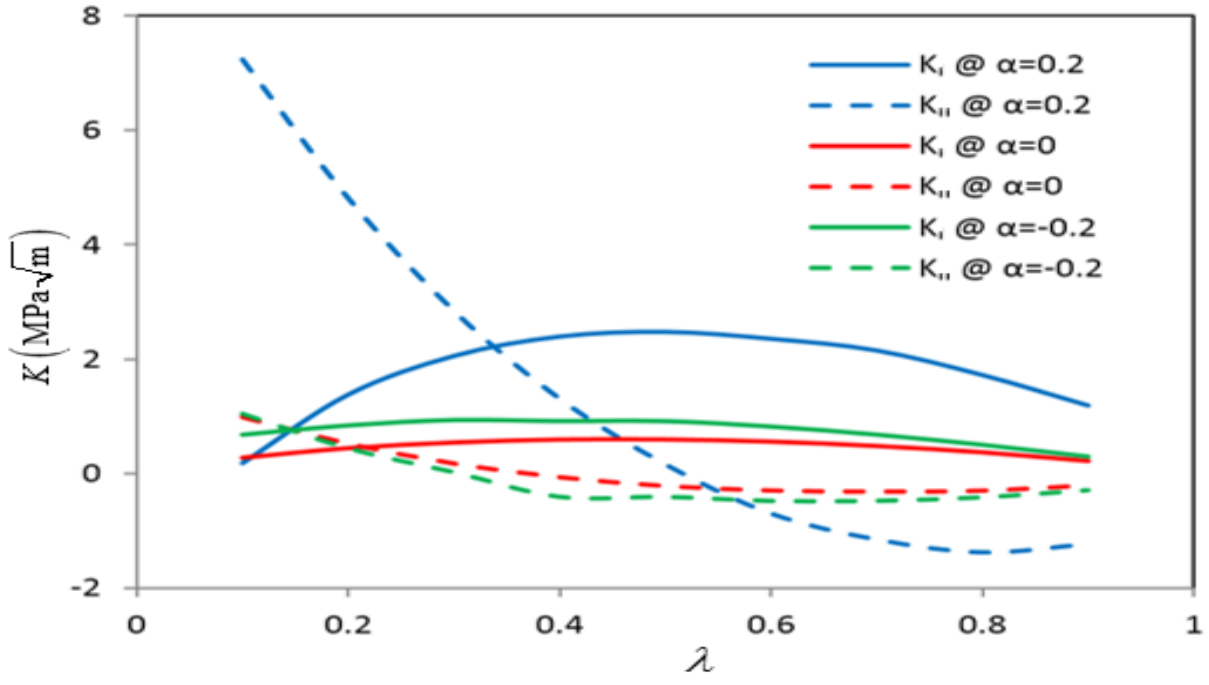

Figure 3.5. The SIFs obtained across the depth of the bottom material

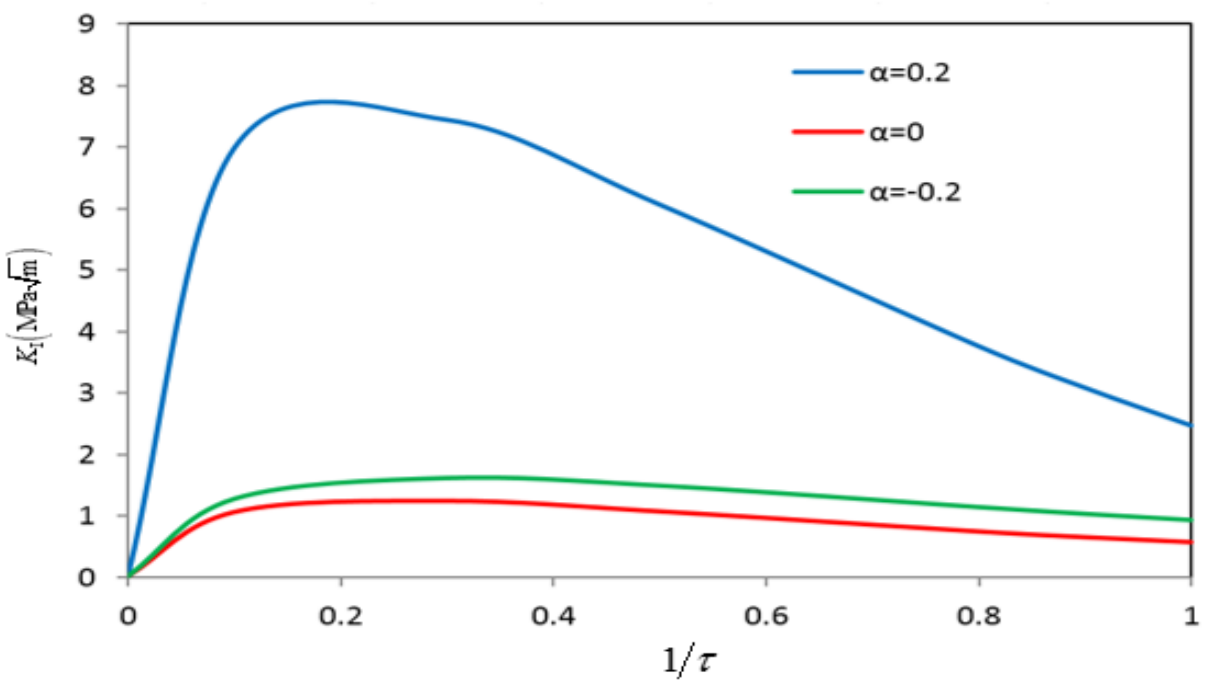

Figure 3.6. Mode I SIF obtained for varying ratios

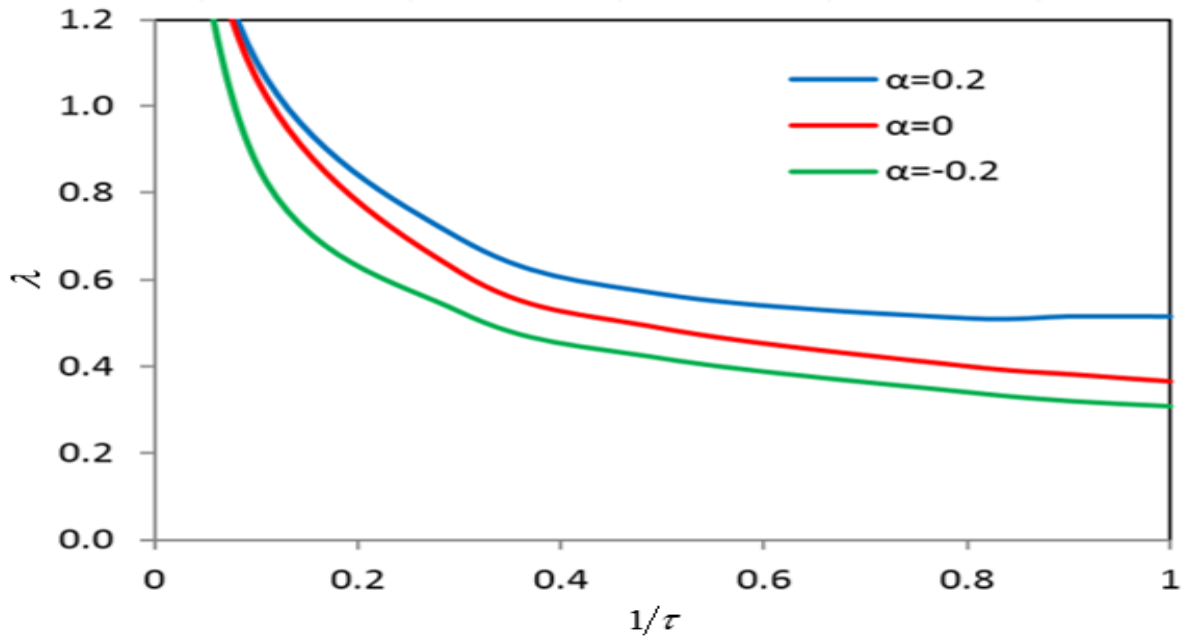

Figure 3.7. SSC depth obtained for varying ratios

4. Specimen Design and Optimization for SCC Study

We have shown the utility of novel bibeam specimens that meet certain stipulated design requirements for studying SCC, and that FEM could be a very good tool for realizing these objectives. The specimen needs to be designed such that the crack reliably starts from a favorable location near this $K_{II} = 0$ path. We develop a Finite Element model to find the relative cracking depth (λ) which gives $K_{II} = 0$ and tune the thickness ratio (h_1/h_2) so that K_I at this location has the desired magnitude of about $0.5 \sim 0.9\, K_{IC}$ for different combinations of the two materials of the specimen.

The materials chosen for this research were only selected based on the availability of material data and required values of α parameter. Four additional bibeam specimen designs were made to obtain K_I that changes with propagation length so that several velocity values rather than a single data point could be obtained. This would be realized by developing bibeam specimens with varying thickness across its length.

Though extended finite element method (XFEM) has gained popularity for its ability to perform FE modeling of cracks without mesh restructuring [33], it has been shown that fracture analysis code FRANC3D interfaced with Abaqus predicts crack growth in a bibeam more accurately than XFEM capability in ABAQUS FE analysis code [34]. FRANC3D [20, 34, 35] code receives a mesh model as input and performs adaptive mesh restructuring to incrementally advance a crack. The SSC propagations for the 5 new specimens were performed using FRANC3D code interfaced with Abaqus. 3D geometry and initial finite element discretization using quadratic quadrilateral elements were done in ABAQUS FE code while the initial crack lengths were specified in the Franc3D code.

The 3-dimensional models for the 5 designs were realized by extruding the 2D model through a thickness of 1mm. Finer discretization of the geometry with a high concentration of elements

near the crack tip was done and stress intensity factors were calculated by the M-integral method [15,16]. The local direction of the crack growth was predicted using the maximum tensile stress criterion.

4.1.SSC in Schott B/Soda-Lime Glass Rectangular Bibeam

We study subcritical crack growth in Soda-lime glass for Design 1. Design 1 is a rectangular bibeam with $1/\tau = 1$ which has the same specimen design used to generate Figure 3.5 but in this section the interest lies in the probable changes in K_I as the crack grows through the entire length of the specimen. The materials chosen for the bibeam were Schott B270 and Soda-lime glass, both having close elastic properties such that $\alpha = 0$. The crack growth through the entire length of the specimen is shown in Figure 4.1.

Figure 4.2 presents the plot of the crack length a against K_I, but the K_I obtained from the design is constant as the crack propagates through the length of the bibeam. This proves that the effect of crack length on K_I in a rectangular beam is the same regardless of the length of the crack.

Figure 4.2 also shows that the magnitude of SSC K_I realizable for bibeam specimen with $1/\tau = 1$ is 0.57MPa.m$^{1/2}$. This value is obtained at the depth of 9.3mm of the bottom material. For required K_I of interest, $1/\tau$ would have to be changed. For this particular study, we obtained $0.76\,K_{IC}$ of Soda-lime glass which is lower than the K_{IC} of Soda-lime (0.75MPa.m$^{1/2}$) but high enough for studying SCC .

Figure 4.1. SSC growth in Design 1

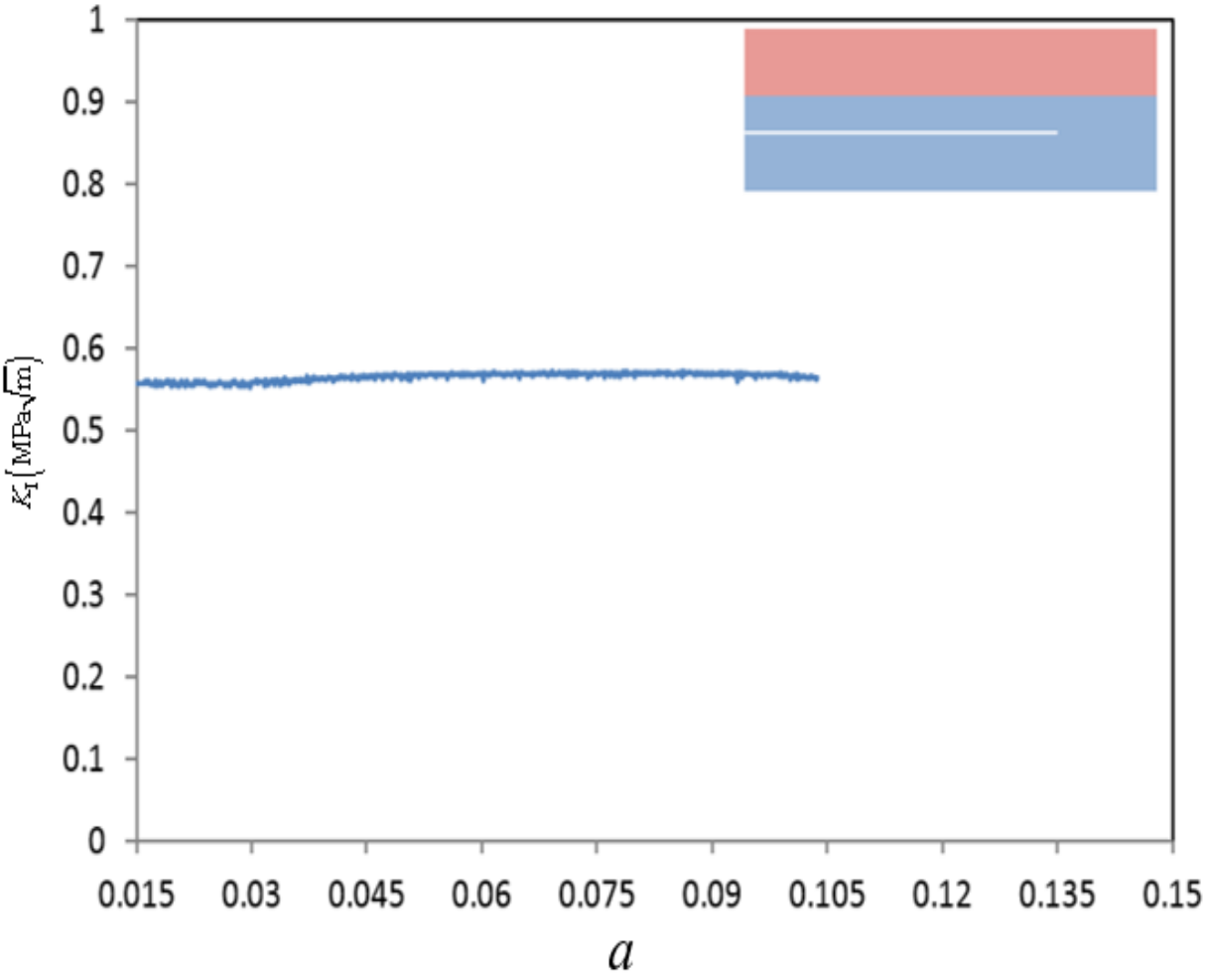

Figure 4.2. K_I at SSC along crack path in a rectangular bimaterial beam

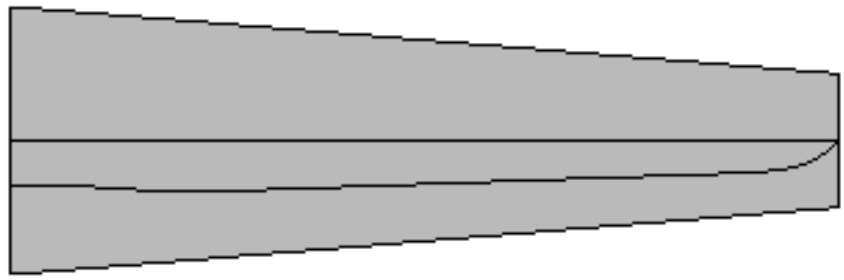

(a)

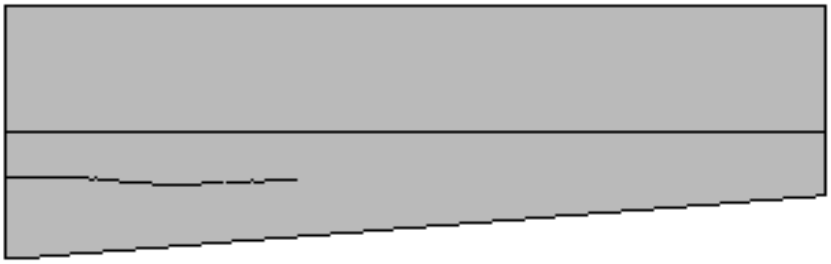

(b)

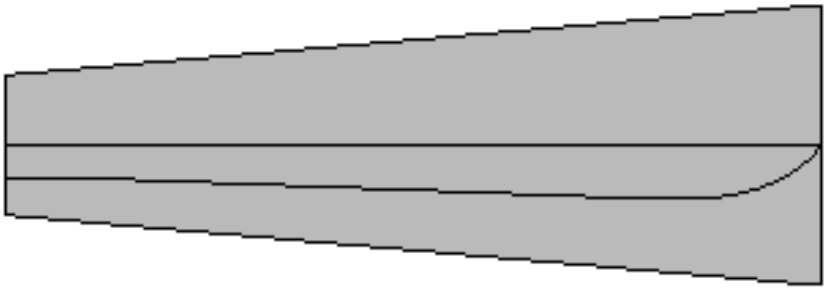

(c)

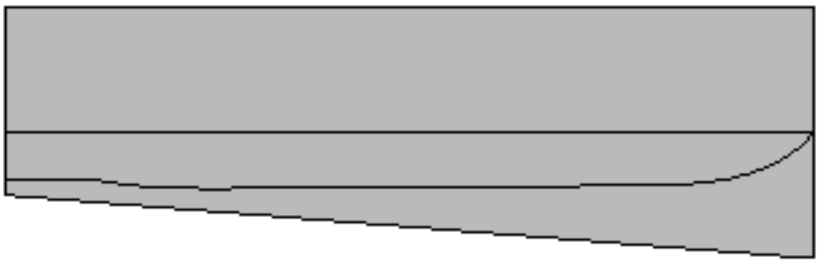

(d)

Figure 4.3. SSC growth in possible specimen designs (a) design 2 (b) design 3 (c) design 4 (d) design 5

4.2. Geometry Design for Non-Constant SIF

The earlier specimen design was modified so that K_I changes with propagation length. Figure 4.3 shows SSC growth across the lengths of the possible specimen designs. Specifically, the dimensions of design 1 was modified to obtain designs 2-5 by reducing either the thickness of the bottom material or both materials thicknesses to half of its original thickness. Since the vertical edges have traction free surface, the traction free boundary condition affects the stress response in the region close to the edges thereby affecting the results obtained for the K_I and K_{II} and would change the direction of the crack growth in Figure 4.4 near the bibeam edges. The results obtained from the zone of influence of the traction boundary conditions with respect to the stress field near the crack tip could be ignored in a SCC growth (SCCG) experiment. SSC modeling assumption are restricted to the region of the specimen which is not influenced by the boundary condition. The K_I values obtained from the crack growth from initial crack length (15mm) to 120mm are considered valid for the design of SCCG.

Designs 2 and 4 have small difference between the lowest K_I and highest K_I while designs 3 and 5 have greater difference between the lowest K_I and highest K_I. The most suitable specimen design choice for investigating SCCG would be design 3 because it has the largest range of K_I from the initial crack length to the final crack length among all the specimen designs considered.

The data obtained from such a design can then populate a range of crack velocity values in Figure 4.4 rather than a single point. If we design the specimen such that K_I decreases with propagation, the design makes it more likely for a notch to survive the bonding process without propagating unstably.

In addition, by observing the K_I value at which the crack tip effectively stops propagating

we can obtain a threshold K_I, analogous to the threshold stress concept in fatigue failure, below which a crack will not propagate even in the presence of water. Increasing K_I can be achieved simply by starting a crack at the opposite end of the specimen. Which would be a replica of design 5.

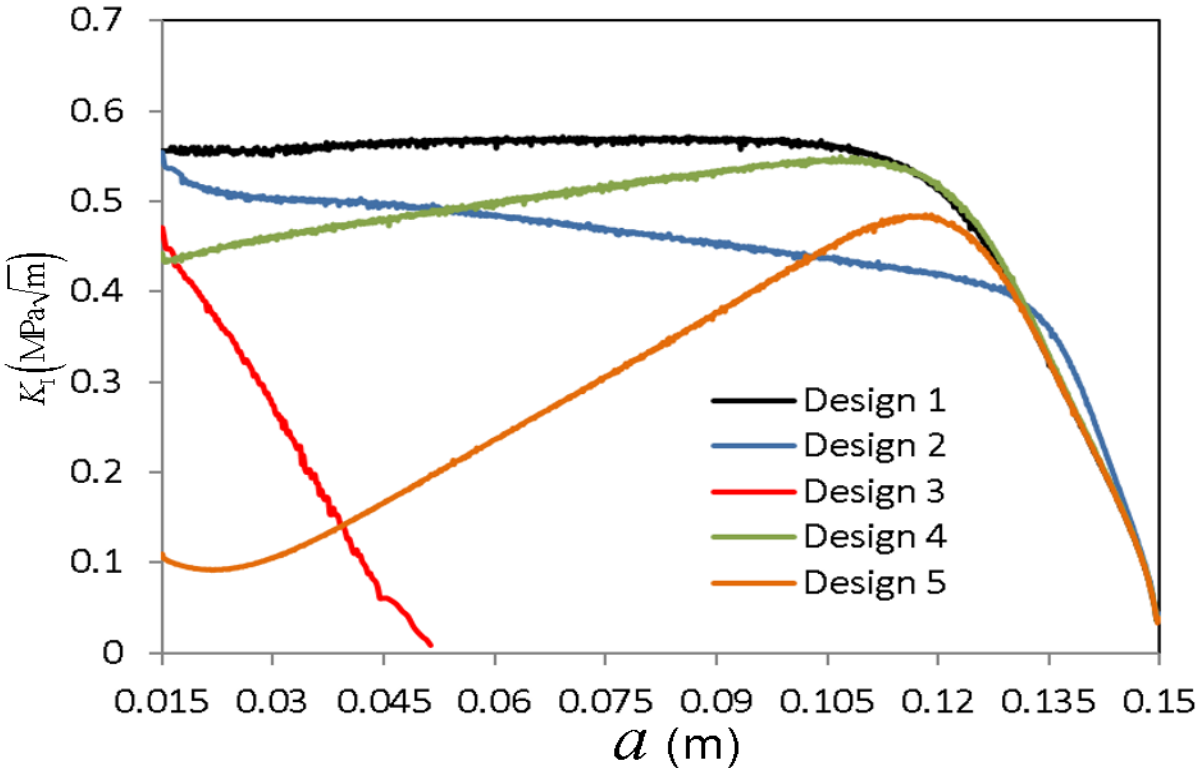

Figure 4.4. The K_I plots along SSC path for possible specimen designs

For study involving bibeam with varied thickness, h_1 represents the maximum edge thickness of the top material and h_2 represents the thickness of the edge with the initial crack. The Relative SSC depths λ of 0.37, 0.34 ,0.37, 0.24 and 0.37 were recorded for Designs 1, 2, 3, 4 and 5. We notice that the lowest λ recorded was from design 4 and the reduction of the thickness of the bottom material on either side does not change the location λ. Rather, λ was reduced when the

thickness of the top material was reduced.

Figure 4.5 shows the mode I SIF that was obtained at the tip of the initial crack in design 3. These results were obtained for initial crack length of 15mm in Soda lime glass and $0.5 \le 1/\tau \ge 1.5$. Increasing $1/\tau$ leads to decreasing values of K_{I}. If initial K_{I} that is greater than $0.76\,K_{\mathrm{IC}}$ is desired, $1/\tau$ would need to be reduced, but reduction beyond 0.75 is unreasonable since the crack would no longer propagates in steady manner.

We plotted the SSC K_{I} across the length of the specimen while reducing $1/\tau$ to the barest minimum in Figure 4.6. The reduction of $1/\tau$ not only produces higher initial SSC K_{I} but also could help produces more data to populate a range of crack velocity values since SSCG velocities for higher K_{I} could be produced.

4.3. Validation of Result with Experiment

The specimen design was validated by performing a SCCG experiment in Soda lime glass deposited in water and air. This experiment was done in Sandia National Laboratories. The design dimensions used were based on $1/\tau = 1$ for bibeam specimen consisting of Schott B glass and Soda lime. Because of the difficulty encountered in creating the initial crack, the initial crack of 4mm and 6mm were used for bibeam in water and air respectively. Figure 4.7 shows the crack in the bibeam deposited in water and air. The crack growth was measured using a camera, and the values collected were plotted against time in Figure 4.8 and Figure 4.9.

The crack initially grows faster at the earlier time than the later time as one would expect because the specimen is designed such that K_{I} reduces with increase in in crack length and smaller K_{I} produces slower crack growth.

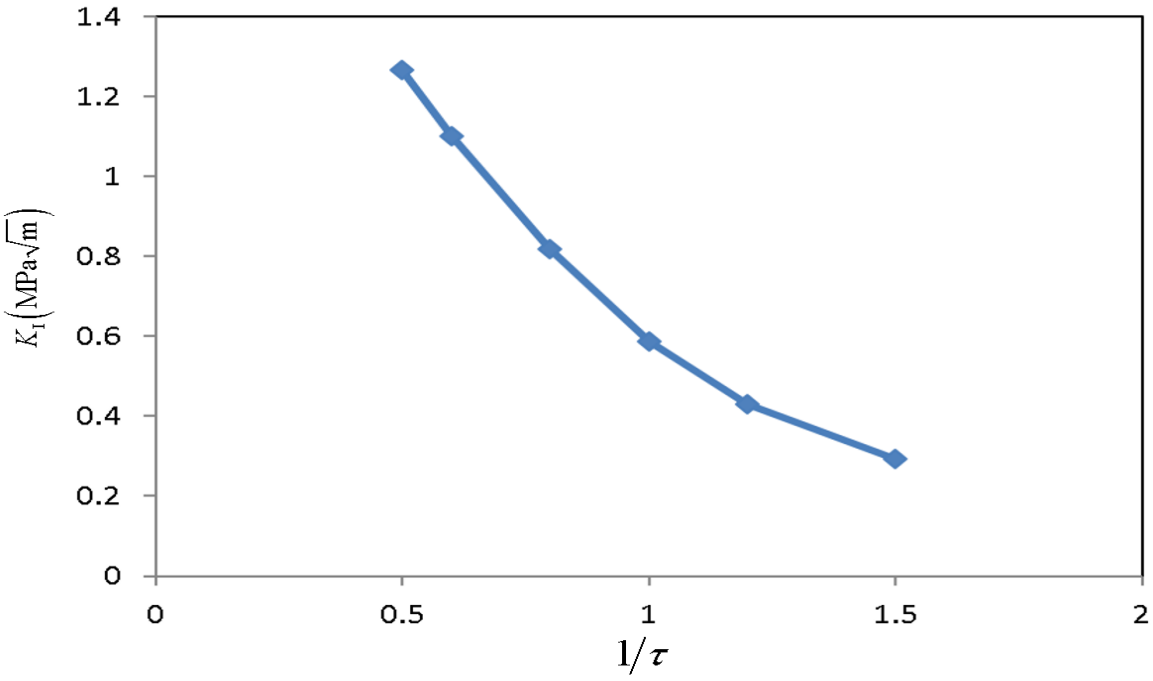

Figure 4.5. Mode I SIF collected for varying geometric ratios of design 3

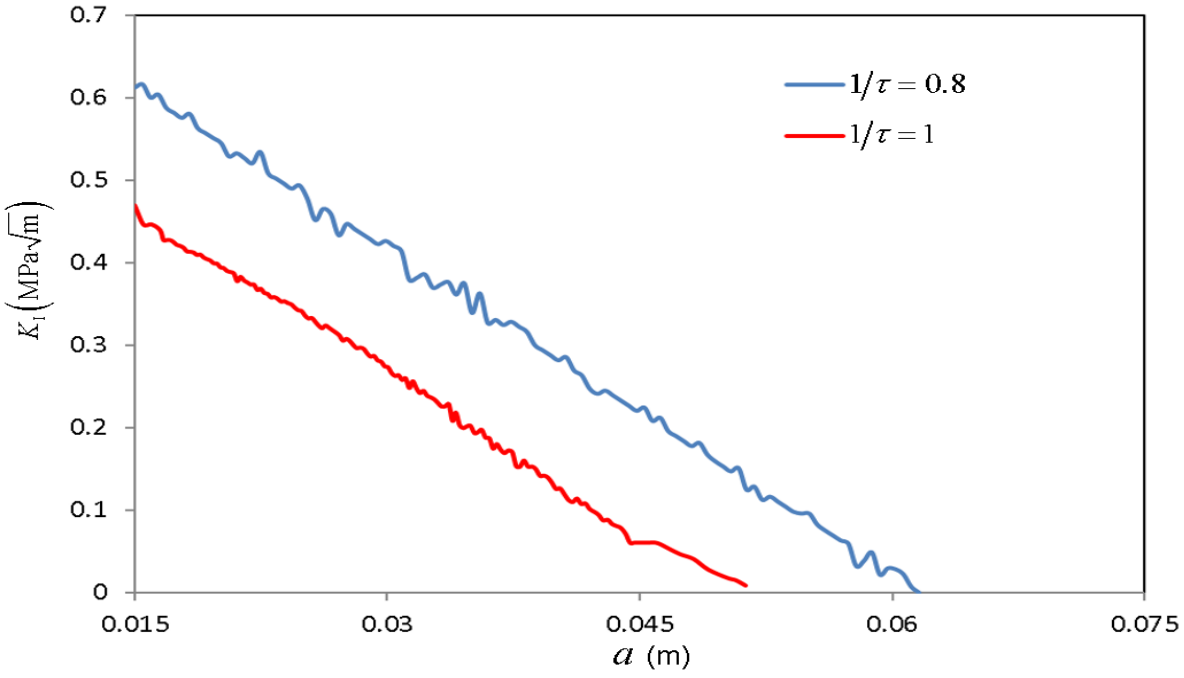

Figure 4.6. The K_I plots along SSC path for design 3

The subcritical crack growth of the bibeam in water and air is plotted in Figure 4.10 and the result obtained from the Bibeam in water compared with the results obtained using Gilman-Wiederdon experiment. The results obtained from our experiment are within the velocity range from 10^{-8} m/s and 10^{-11} m/s. This experiment could capture beyond this range for other SCCG analysis in this material or other materials. In fact, these experiments are still running and we continue to probe the lower tail of the crack velocity curve. The data obtained from bibeam specimen in water also compares well the published data [36]. This makes this specimen design well suited for investigating SCCG. We also note that the crack growth rates in water are approximately 10x slower in air.

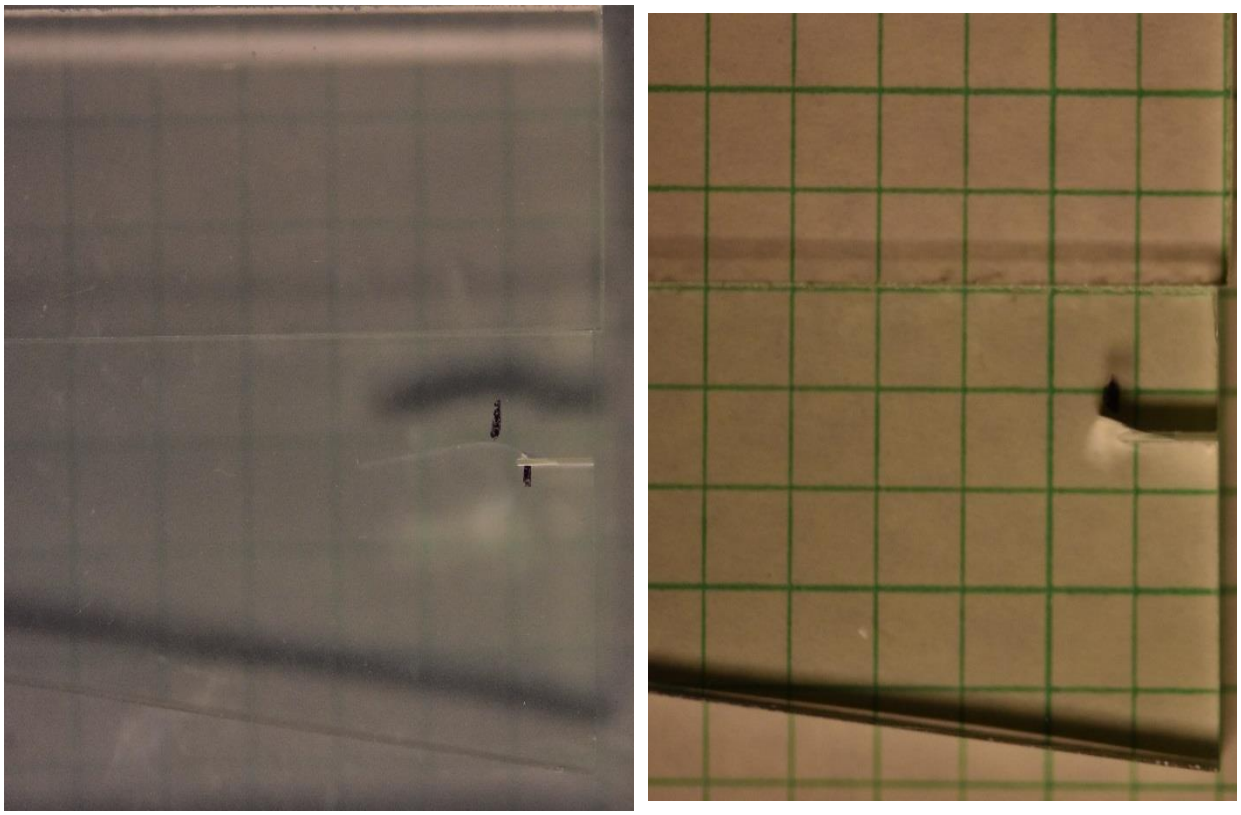

(a) (b)

Figure 4.7. SCCG in soda lime glass (a) medium: water (b) medium: air

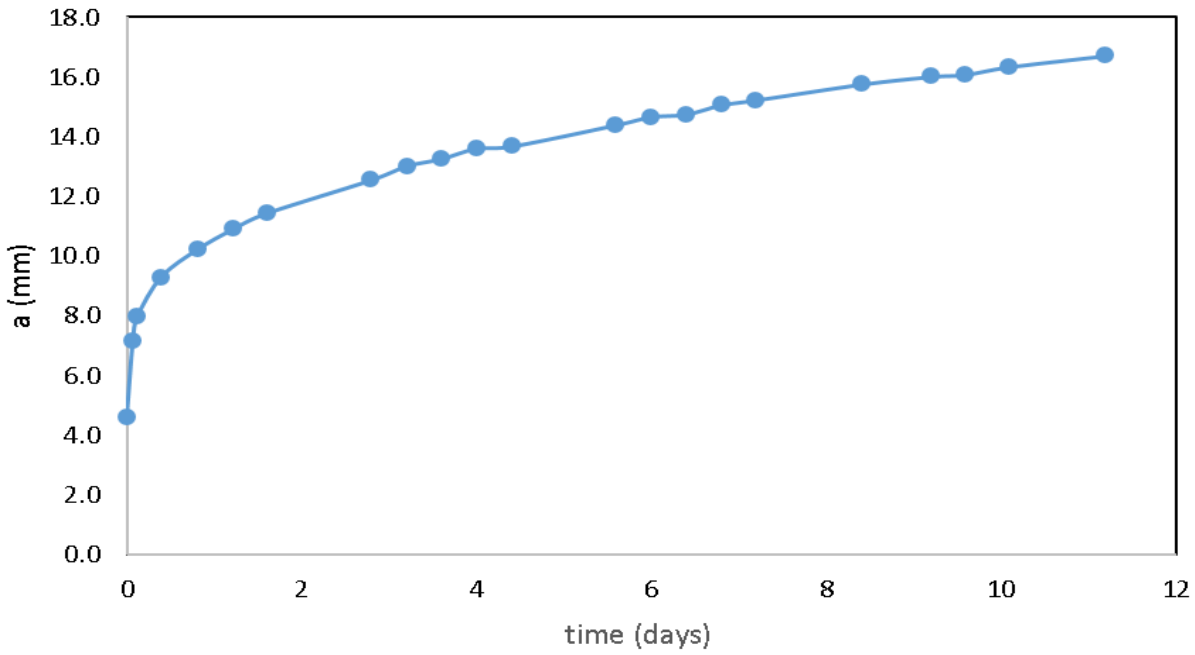

Figure 4.8. SCCG data collected for Soda lime glass in water

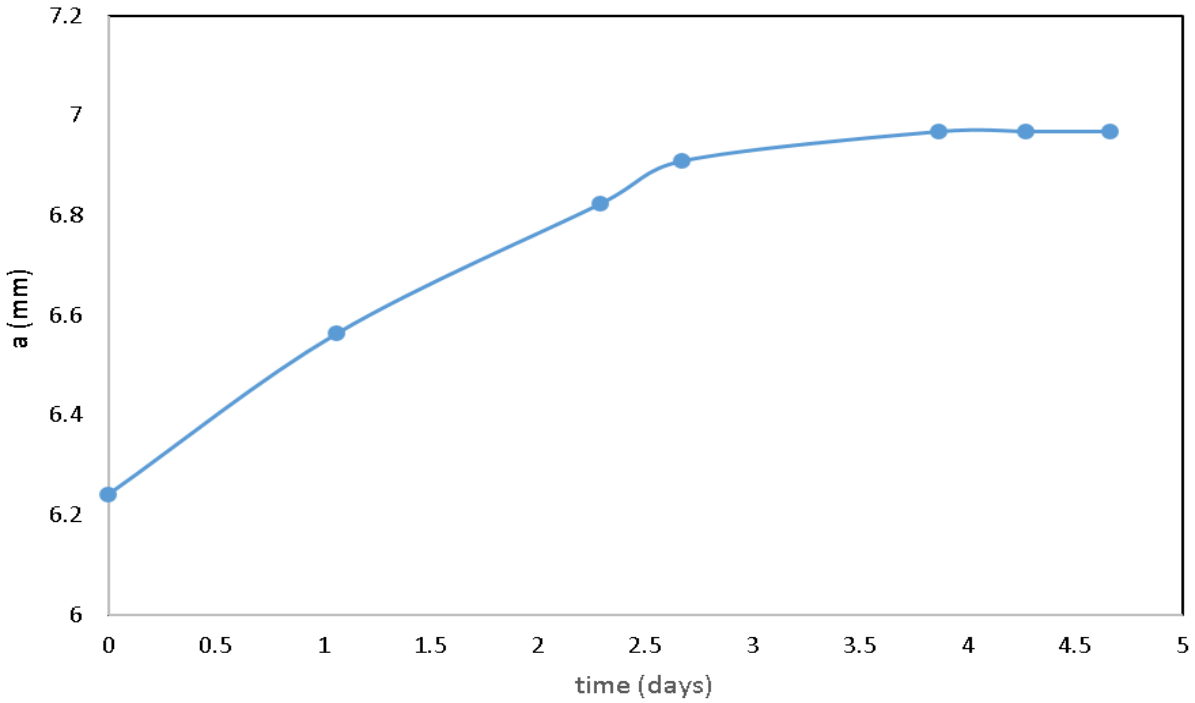

Figure 4.9. SCCG data collected for Soda lime glass in air

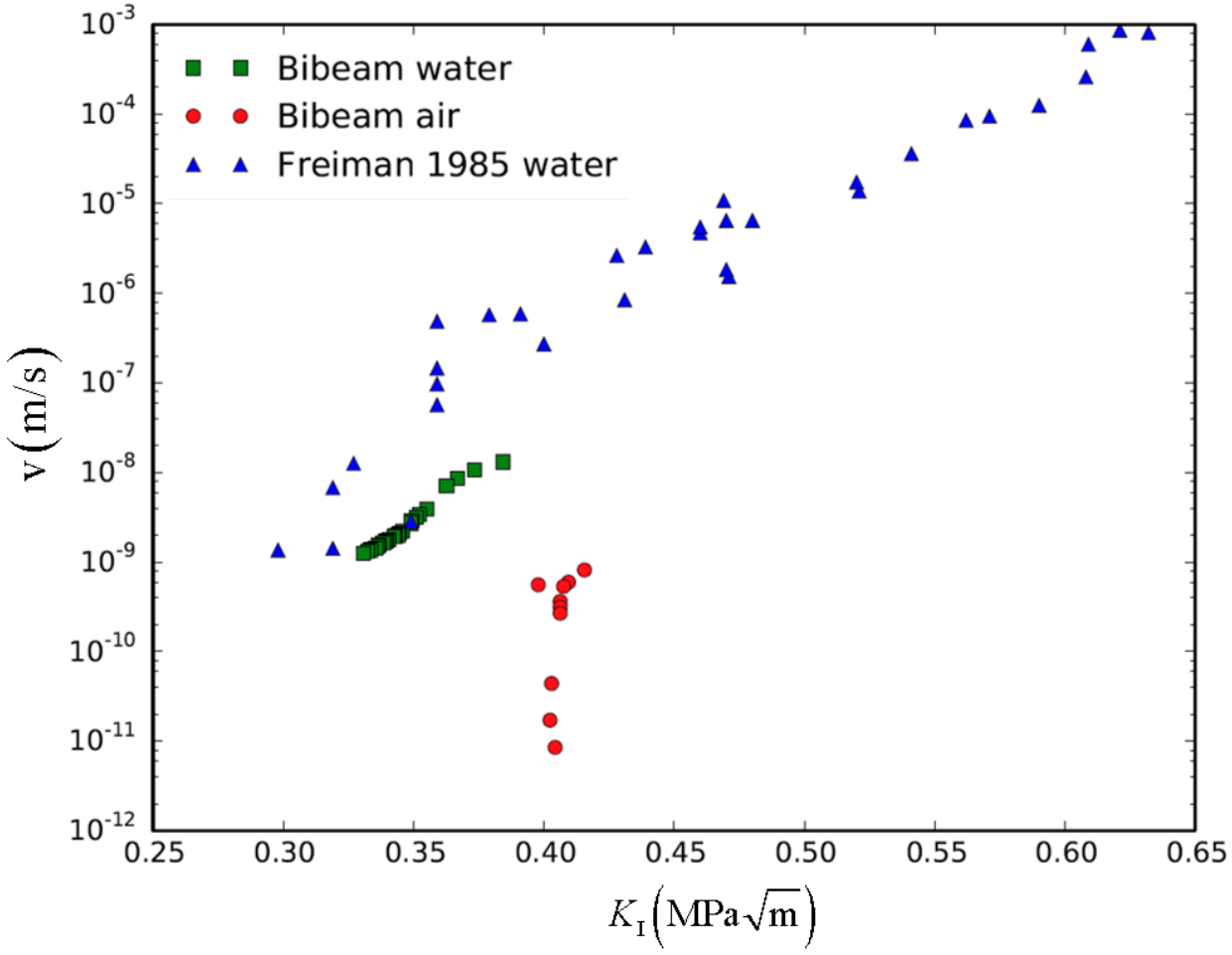

Figure 4.10. Comparison of results with existing data.

5. Conclusion

SCC is an important factor in determining service life or shelf life of a component. In the past, SCC has been studied under a variety of conditions, but specimens have always required a load to be externally applied. The most common setup requires a double cantilever beam specimen subjected to a constant external loading or bending moment were crack extension are measured as a function of time using optical equipment. Crack velocities that range from 10^{-10} to 10^{-2} m/s could be collected through this method and constant applied load are maintained during measurements. We propose a new type of specimen consisting of a bimaterial beam where the two materials have slightly different coefficient of thermal expansions (CTEs) to study SCC. If both materials are glass, they can be diffusion bonded at a temperature of around 400-600°C. As they cool to room temperature the two materials will contract by different amounts according to their CTE values. Because they are constrained to be the same length along the interface, this puts the composite beam in bending with tensile stresses in the material with the smaller CTE value.

FEM was employed for developing and analysis of these specimens. To validate the FEM method, analytical method described for studying steady state cracking in film deposited on a substrate was revisited to compare the predictions of SSC depth and SSC K_I.

Both methods were extended to bibeam specimens, but the results show that though both methods produced the same results for SSC depth, the K_I obtained at these depths vary. This was attributed to validity of the assumptions made for film/substrate specimen which may no longer hold true for bibeam specimen. Also, a recommended conservative value of angle $\omega = 52^0$ was used for the entire simulations which could contribute to the error in the analytical model.

Most of the designs considered in these analyses were for bibeam where there is almost no elastic mismatch ($\alpha = 0$) between the top material and bottom material. We did explore the effect of change in α when need arises. Because of the readily availability of the Schott B glass and Soda

lime, these materials were chosen for the top and bottom materials to produce $\alpha = 0$ condition for the bibeam

We showed that a rectangular bibeam specimen could only produce a non-varying SIF as the crack propagates. The Specimen dimensions were optimized by studying four more specimens and results shows that the Design 3 is the best design. This is because the data obtained from such a design can then populate a range of crack velocity values rather than a single point obtained from Design 1. If we design the specimen such that K_I decreases with propagation, it makes it more likely a notch will survive the bonding process without propagating unstably.

The specimen design was validated by performing an experiment for SCCG in Soda lime glass deposited in water and air. The results obtained from our experiment are within the velocity range from 10^{-8} m/s and 10^{-11}m/s. This experiment could capture beyond this range for other SCCG analysis in this material or other materials. In fact, these experiments are still running and we continue to probe the lower tail of the crack velocity curve. The data obtained from bibeam specimen in water also compares well the published data. This makes this specimen design well suited for investigating SCCG. We also note that the crack growth rates in water are approximately 10x slower in air.

References

1. **Heathcote, T.A., *The military in British India: the development of British land forces in South Asia, 1600-1947*. 1995: Manchester University Press.**
2. **Nicolet-Monnier, M. and A.V. Gheorghe, *Pipelines and Storage Tanks for Gases and Petroleum Products*, in *Quantitative Risk Assessment of Hazardous Materials Transport Systems*. 1996, Springer. p. 181-200.**
3. **Lichtenstein, A.G., *The silver bridge collapse recounted.* Journal of performance of constructed facilities, 1993. 7(4): p. 249-261.**
4. **Maczak, J., *The concept of the distributed diagnostic system for structural health monitoring of critical elements of infrastructure objects*, in *Asset Condition, Information Systems and Decision Models*. 2012, Springer. p. 125-131.**
5. **Freiman, S., *Effects of chemical environments on slow crack growth in glasses and ceramics.* Journal of Geophysical Research: Solid Earth, 1984. 89(B6): p. 4072-4076.**
6. **Freiman, S.W., S.M. Wiederhorn, and J.J. Mecholsky Jr, *Environmentally enhanced fracture of glass: a historical perspective.* Journal of the American Ceramic Society, 2009. 92(7): p. 1371-1382.**
7. **Wiederhorn, S., *Moisture assisted crack growth in ceramics.* International Journal of Fracture Mechanics, 1968. 4(2): p. 171-177.**
8. **Wiederhorn, S., *Influence of Water Vapor on Crack Propagation in Soda-Lime Glass.* Journal of the American Ceramic Society, 1967. 50(8): p. 407-414.**
9. **Wiederhorn, S. and L. Bolz, *Stress corrosion and static fatigue of glass.* Journal of the American Ceramic Society, 1970. 53(10): p. 543-548.**
10. **Smedskjaer, M.M. and M. Bauchy, *Sub-critical crack growth in silicate glasses: Role of network topology.* Applied Physics Letters, 2015. 107(14): p. 141901.**
11. **Ronchetti, C., et al., *Stress-corrosion failure mechanisms in soda–lime silica glass.* Engineering Failure Analysis, 2013. 35: p. 427-438.**
12. **Raja, V. and T. Shoji, *Stress corrosion cracking: theory and practice*. 2011: Elsevier.**
13. **Freiman, S., *Fracture mechanics of glass.* Glass: Science and Technology, 2012. 5: p. 21-78.**
14. **Chevalier, J., C. Olagnon, and G. Fantozzi, *Subcritical Crack Propagation in 3Y-TZP Ceramics: Static and Cyclic Fatigue.* Journal of the American Ceramic Society, 1999. 82(11): p. 3129-3138.**
15. **Bunker, B., *Molecular mechanisms for corrosion of silica and silicate glasses.* Journal of Non-Crystalline Solids, 1994. 179: p. 300-308.**
16. **Gilman, J.J., *Direct measurements of the surface energies of crystals.* Journal of Applied Physics, 1960. 31(12): p. 2208-2218.**
17. **Nakayama, J., *Direct measurement of fracture energies of brittle heterogeneous materials.* Journal of the American Ceramic Society, 1965. 48(11): p. 583-587.**
18. **Rountree, C.L., *Recent progress to understand stress corrosion cracking in sodium***

borosilicate glasses: linking the chemical composition to structural, physical and fracture properties. **Journal of Physics D: Applied Physics, 2017. 50(34): p. 343002.**

19. **Ciccotti, M., *Stress-corrosion mechanisms in silicate glasses.* Journal of physics D: Applied physics, 2009. 42(21): p. 214006.**
20. **Aduloju, S., et al., *Designing Brittle Fracture Specimens to Investigate Environmentally Assisted Crack Growth*, in *Fracture, Fatigue, Failure and Damage Evolution, Volume 7*. 2018, Springer. p. 25-33.**
21. **Matsinos, E., *Steady-state cracking in brittle substrates beneath adherent films: revisited.* arXiv preprint arXiv:1111.6152, 2011.**
22. **Suo, Z. and J.W. Hutchinson, *Steady-state cracking in brittle substrates beneath adherent films.* International Journal of Solids and Structures, 1989. 25(11): p. 1337-1353.**
23. **Evans, A., M. Drory, and M. Hu, *The cracking and decohesion of thin films.* Journal of Materials Research, 1988. 3(5): p. 1043-1049.**
24. **Argon, A.S., et al., *Intrinsic toughness of interfaces between SiC coatings and substrates of Si or C fibre.* Journal of Materials Science, 1989. 24(4): p. 1207-1218.**
25. **Hu, M., M.D. Thouless, and A.G. Evans, *The decohesion of thin films from brittle substrates.* Acta Metallurgica, 1988. 36(5): p. 1301-1307.**
26. **Drory, M.D., M.D. Thouless, and A.G. Evans, *On the decohesion of residually stressed thin films.* Acta metallurgica, 1988. 36(8): p. 2019-2028.**
27. **Thouless, M., et al., *The edge cracking and spalling of brittle plates.* Acta Metallurgica, 1987. 35(6): p. 1333-1341.**
28. **Negus, M., et al., *Designing Brittle Fracture Specimens to Investigate Environmentally Assisted Crack Growth*. 2016, Sandia National Laboratories (SNL-NM), Albuquerque, NM (United States).**
29. **Hutchinson, J.W. and Z. Suo, *Mixed mode cracking in layered materials.* Advances in applied mechanics, 1991. 29: p. 63-191.**
30. **Schmauder, S. and M. Meyer, *Correlation between Dundurs' parameters and elastic constants.* Z. Metallkd, 1992. 83(7): p. 524-527.**
31. **Bogy, D., *On the problem of edge-bonded elastic quarter-planes loaded at the boundary.* International Journal of Solids and Structures, 1970. 6(9): p. 1287-1313.**
32. **Chen, J. and S. Bull, *Approaches to investigate delamination and interfacial toughness in coated systems: an overview.* Journal of Physics D: Applied Physics, 2010. 44(3): p. 034001.**
33. **Belytschko, T., R. Gracie, and G. Ventura, *A review of extended/generalized finite element methods for material modeling.* Modelling and Simulation in Materials Science and Engineering, 2009. 17(4): p. 043001.**
34. **Grutzik, S.J. and E.D. Reedy, *Development of Glass/Steel Bibeam Specimen for Study***

of Brittle Crack Path Stability, in *Experimental and Applied Mechanics, Volume 4*. 2017, Springer. p. 59-66.

35. Grutzik, S.J. and E.D. Reedy, *Crack Path Selection in Thermally Loaded Borosilicate/Steel Bibeam Specimen.* Experimental Mechanics, 2018. 58(1): p. 1-10.
36. Freiman, S.W., G.S. White, and E.R. Fuller, *Environmentally Enhanced Crack Growth in Soda-Lime Glass.* Journal of the American Ceramic Society, 1985. 68(3): p. 108-112.

Appendices

Appendix A: Analytical Prediction of SSC in Film-Substrate System

```
%%    Steady state crack growth in film-substrate systems
% Code for chapter 2
%code written by Sunday Aduloju                    07-04-2016
% updated    01/29/2018
%%%%%%%%%%%%%%%%%%%%%%%%%%%%%%%%%%%%%%%%%%%%%%%%%%%%%%%%%%%%%%%%%%%%%%%%

clear
clc

%dundurs parameters
beta=0;
alpha=0;%(F*(k2+1)-
(k1+1))/(F*(k2+1)+(k1+1));%0.8%*****************************************************************
omega=52;%%
sigma=3.5156e+07; %Misfit stress in MPa
%% geometric properties
h= 25.4e-4;%0.001; %film thickness in meters
h1=25.4e-4; %Initial Crack depth in meters
hs=25.4e-3;%0.01;%Substrate thickness in meters
tau=hs/h;%10 %Substrate/film thickness ratio%%**************************************************
tau_inv=inv(tau); % inverse of tau
c2=1; %assume c2= 1 since it cancels each other when you find ERRratio
lamda=h1/h; %relative crack depth
%%%%%%%%%%%%%%%%%%%%%%%%%%%%%%%%%%%%%%%%%%%%%%%%%%%%%%%%%%%%%%%%%%%%%%%%
```

```
[lamda, enforceDiff,K1,K2,A_fa, A_fb,I_fa, I_fb,delta_fa,delta_fb,omegaC ] = Zero_Enforcement(lamda,alpha,tau,
sigma,h, omega);
%InitialCrack
fprintf('The initial crack results are: \n');
fprintf('lamda1 = %d, enforceDiff = %d      Stress intensity factors KI = %d, KII = %d, omegaC = %d
\n\n',lamda,enforceDiff, K1,K2,omegaC);
lamda=1.05; %stable crack depth/film thickness ratio
hc=lamda*h; %stable crack depth
%%%%%%%%%%%%%%%%%%%%%%%%%%%%%%%%%%%%%%%%%%%%%%%%%%%%%%%%%%%%%%%%%%%%%%%%%%%%%%
%%%%%%%%%%%%%%%%%%%%%%%%%%%%%%%%%%%%%%%%%%%%%%%%%%%%%%%%%%%%%%%%%%%%%%%%%%%%%%
%%%%%%%%%%%%%%%%%%%%%%%%%%%%%%%%%%%%%%%%%%%%%%%%%%%%%%%%%%%%%%%%%%%%%%%%%%%%%%
[lamda, enforceDiff,K1,K2,A_fa, A_fb,I_fa, I_fb,delta_fa,delta_fb ] = Zero_Enforcement(lamda,alpha,tau, sigma,h,
omega);
omegaC=K1/(sigma*h^0.5);
ERR= (c2*sigma^2*h/16)*(1/A_fb+(lamda-delta_fb+0.5)^2/I_fb-1/A_fa-(tau-delta_fa+0.5)^2/I_fa)%Energy
release rate
fprintf('The settings for stable crack are: \n');
fprintf('        alpha = %f,         tau = %f,    omega = %f,    lamda = %f\n',alpha,tau,omega,lamda);
fprintf('The results are: \n');
fprintf(' tau_inv = %f, enforceDiff = %d,    hc = %f \n',tau_inv,enforceDiff,hc);
fprintf(' Stress intensity factor K1 = %d, omegaC = %d', K1,omegaC);

%z=(1/A+(lamda-delta+0.5)^2/I-1/A_not-(tau-delta_not+0.5)^2/I_fb)
lamdai=0;
lamda=lamdai;
```

```
[lamda, enforceDiff,K1,K2,A_fa, A_fb,I_fa, I_fb,delta_fa,delta_fb ] = Zero_Enforcement(lamda,alpha,tau, sigma,h, omega);
ERRi= (c2*sigma^2*h/16)*(1/A_fb+(lamdai-delta_fb+0.5)^2/I_fb-1/A_fa-(tau-delta_fa+0.5)^2/I_fa);%Energy release rate
%ERRinterface;
ERRratio=ERR/ERRi;
%y=z/b
fprintf(' and ERRratio= %f \n\n',    ERRratio);
%%%%%%%%%%%%%%%%%%%%%%%%%%%%%%%%%%%%%%%%%%%%%%%%%%%%%%%%%%%%%%%%%%%%
%%%%%%%%%%%%%%%%%%%%%%%%%%%%%%%%%%%%%%%%%%%%%%%%%%%%%%%%%%%%%%%%%%%%
%%%%%%%%%%%%%%%%%%%%%%%%%%%%%%%%%%%%%%%%%%%%%%%%%%%%%%%%%%%%%%%%%%%%
function [lamda, enforceDiff,K1,K2,A_fa, A_fb,I_fa, I_fb,delta_fa,delta_fb,omegaC ] = Zero_Enforcement(lamda,alpha,tau, sigma,h, omega);
%function [ElemK,ElemF,hr] = NL_Elem63_1dDGF03_Complete(iter,mateprop,ul,xl,hr,nh1,nh2,nh3,ndf,ndm,nst,nel,nelP,nen,sigmaC,delC)%,zeta)
sigmaE=(1+alpha)/(1-alpha); %the stiffness ratio
delta_fb=(lamda^2+2*sigmaE*lamda+sigmaE)/(2*(lamda+sigmaE));
delta_fa=(tau^2+2*sigmaE*tau+sigmaE)/(2*(tau+sigmaE));
P1=sigma*h;
P3=sigma*h;
M1=sigma*h^2*(0.5 +lamda-delta_fb);
M3=sigma*h^2*(0.5 +tau-delta_fa);
%% Cross-section and moments
%for upper beam far behind the crack tip
A_fb=lamda+sigmaE; %dimensionless effective cross-section
```

```
I_fb=(sigmaE*(3*(delta_fb-lamda)^2-3*(delta_fb-lamda)+1)+3*delta_fb*lamda*(delta_fb-lamda)+lamda^3)/3; %
moment of inertia per unit width
% for the layer far ahead of the crack tip
A_fa=tau+sigmaE; %dimensionless effective cross-section
I_fa=(sigmaE*(3*(delta_fa-tau)^2-3*(delta_fa-tau)+1)+3*delta_fa*tau*(delta_fa-tau)+tau^3)/3; % moment of
inertia per unit width
C1=A_fb/A_fa;
C2=(A_fb/I_fa)*((tau-delta_fa)-(lamda-delta_fb));
C3=I_fb/I_fa;
P=sigma*h*(1-C1-C2*(0.5+tau-delta_fa));
M=sigma*h^2*((0.5+lamda-delta_fb)-C3*(0.5+tau-delta_fa));
U=(A_fb*(tau-lamda)^3)/((tau-lamda)^3 + A_fb*(tau-lamda)^2 + 12*A_fb*(delta_fb+(tau-lamda)/2)^2);
V= (I_fb*(tau-lamda)^3)/((tau-lamda)^3 + 12*I_fb);
%%%%%%%%%%%%%%%%%%%%%%
% U=(A_fa*(tau-lamda)^3)/((tau-lamda)^3 + A_fa*(tau-lamda)^2 + 12*A_fa*(delta_fa+(tau-lamda)/2)^2);
% V= (I_fa*(tau-lamda)^3)/((tau-lamda)^3 + 12*I_fa);
gamma=asind( (12*(delta_fb+(tau-lamda)/2)/(tau-lamda)^3)*sqrt(U*V));
enforceLeft=(cosd(omega+gamma))/sind(omega);
enforceRight=sqrt(V/U)*(P*h/M);
enforceDiff=enforceRight-enforceLeft;
%% %%%%%%%%%%%%%%%%%%%%%%%%%%%%%%%%%%%%%%%%%%%%%%%%%%%%%%%%%%
%%%%%%%%%%%%%%%%%%%%%%%%%%%%%%%%%%%%%%%%%%%%%%%%%%%%%%%%%%%%%%
K1=((P/sqrt(2*U*h))*cosd(omega))+ (M/sqrt(2*V*h^3))*sind(omega+gamma);
K1_reduced= (P/sqrt(2*h*A_fb))*cosd(omega) + (M/sqrt(2*h^3*I_fb))*sind(omega);
omegaC=K1/(sigma*h^0.5);
K2=((P/sqrt(2*U*h))*sind(omega))+ (M/sqrt(2*V*h^3))*cosd(omega+gamma);
```

Appendix B: Analytical Prediction of SSC in Bibeam Specimen

```
%%    Steady state crack growth in bibeam
% Code for chapter 3
% written by Sunday Aduloju                    07-14-2016
% updated    01/29/2018


clear
clc
%%
%% %%%for plane strain, s=1, for plane stress, s=2
s=1; % plane strain
%% Material properties
%Film Material Name = Schott B 270
E1=71.5e9; %Elastic modulus of film
v1=0.22; %poisson ratio of the film
CTE1=9.7357e-6;%coefficient of thermal expansion of the film
%Substrate Material name = sodalime glass
E2=74e9; % Elastic modulus of Substrate
v2=0.24; %poisson ratio of the substrate
CTE2=8.9283e-6;%coefficient of thermal expansion of the Substrate
%%
%% Temperature
Tb=500+273; %bonding temperature in K
Tr=25 +273;    %room temperature in K
%% Shear Modulus
```

```
G1=E1/(2*(1+v1)); %Shear Modulus of the Film

G2=E2/(2*(1+v2)); %Shear Modulus of the Substrate

%% for plane strain

if s==1

    k1=3-4*v1; %film variable to calculate dundurs' parameter

     k2=3-4*v2; % substrate variable to calculate dundurs' parameter

%% for plane stress

else

    k1=(3-v1)/(1+v1); %film variable to calculate dundurs's parameter

    k2=(3-v2)/(1+v2); % substrate variable to calculate dundurs parameter

end

c1=(k1+1)/G1;

c2=(k2+1)/G2;

F=G1/G2;

%%

%dundurs parameters

beta=0;

alpha=(F*(k2+1)-(k1+1))/(F*(k2+1)+(k1+1));%0.8%******************

%% %%%%%%%%

omega=52;%%*****************************************************************************

sigma=((CTE1-CTE2)*(Tb-Tr)*E1)/(1-v1);%Misfit stress in MPa

%%

%% geometric properties

h= 25.4e-4;%0.001; %film thickness in meters

h1=25.4e-4; %Initial Crack depth in meters

hs=25.4e-3;%0.01;%Substrate thickness in meters
```

```
tau=hs/h;%10 %Substrate/film thickness ratio%%**************************************************
tau_inv=inv(tau); % inverse of tau
lamda=h1/h; %relative crack depth
  [lamda, enforceDiff,K1,K2,A_fa, A_fb,I_fa, I_fb,delta_fa,delta_fb,omegaC ] =
Zero_Enforcement(lamda,alpha,tau, sigma,h, omega);
%%
%InitialCrack
fprintf('The initial crack results are: \n');
fprintf('lamda1 = %d, enforceDiff = %d      Stress intensity factors KI = %d, KII = %d, omegaC = %d
\n\n',lamda,enforceDiff, K1,K2,omegaC);
lamda=1.05; %stable crack depth/film thickness ratio
hc=lamda*h; %stable crack depth
[lamda, enforceDiff,K1,K2,A_fa, A_fb,I_fa, I_fb,delta_fa,delta_fb ] = Zero_Enforcement(lamda,alpha,tau, sigma,h,
omega);
omegaC=K1/(sigma*h^0.5);
ERR= (c2*sigma^2*h/16)*(1/A_fb+(lamda-delta_fb+0.5)^2/I_fb-1/A_fa-(tau-delta_fa+0.5)^2/I_fa)%Energy
release rate
fprintf('The settings for stable crack are: \n');
fprintf('       alpha = %f,       tau = %f,    omega = %f,    lamda = %f\n',alpha,tau,omega,lamda);
fprintf('The results are: \n');
fprintf(' tau_inv = %f, enforceDiff = %d,    hc = %f \n',tau_inv,enforceDiff,hc);
fprintf(' Stress intensity factor K1 = %d, omegaC = %d', K1,omegaC);
%z=(1/A+(lamda-delta+0.5)^2/I-1/A_not-(tau-delta_not+0.5)^2/I_fb)
lamdai=0;
lamda=lamdai;
```

```
[lamda, enforceDiff,K1,K2,A_fa, A_fb,I_fa, I_fb,delta_fa,delta_fb ] = Zero_Enforcement(lamda,alpha,tau, sigma,h,
omega);
ERRi= (c2*sigma^2*h/16)*(1/A_fb+(lamdai-delta_fb+0.5)^2/I_fb-1/A_fa-(tau-delta_fa+0.5)^2/I_fa);
%Energy release rate
%ERRinterface;
ERRratio=ERR/ERRi;
%y=z/b
%
%%


fprintf(' and ERRratio= %f \n\n',    ERRratio);
function [lamda, enforceDiff,K1,K2,A_fa, A_fb,I_fa, I_fb,delta_fa,delta_fb,omegaC ] =
Zero_Enforcement(lamda,alpha,tau, sigma,h, omega);
sigmaE=(1+alpha)/(1-alpha); %the stiffness ratio
delta_fb=(lamda^2+2*sigmaE*lamda+sigmaE)/(2*(lamda+sigmaE));
delta_fa=(tau^2+2*sigmaE*tau+sigmaE)/(2*(tau+sigmaE));
P1=sigma*h;
P3=sigma*h;
M1=sigma*h^2*(0.5 +lamda-delta_fb);
M3=sigma*h^2*(0.5 +tau-delta_fa);
%%
%% Cross-section and moments
%for upper beam far behind the crack tip
A_fb=lamda+sigmaE; %dimensionless effective cross-section
I_fb=(sigmaE*(3*(delta_fb-lamda)^2-3*(delta_fb-lamda)+1)+3*delta_fb*lamda*(delta_fb-lamda)+lamda^3)/3; %
moment of inertia per unit width
```

```
% for the layer far ahead of the crack tip
A_fa=tau+sigmaE; %dimensionless effective cross-section
I_fa=(sigmaE*(3*(delta_fa-tau)^2-3*(delta_fa-tau)+1)+3*delta_fa*tau*(delta_fa-tau)+tau^3)/3; % moment of inertia per unit width
C1=A_fb/A_fa;
C2=(A_fb/I_fa)*((tau-delta_fa)-(lamda-delta_fb));
C3=I_fb/I_fa;
P=sigma*h*(1-C1-C2*(0.5+tau-delta_fa));
M=sigma*h^2*((0.5+lamda-delta_fb)-C3*(0.5+tau-delta_fa));
U=(A_fb*(tau-lamda)^3)/((tau-lamda)^3 + A_fb*(tau-lamda)^2 + 12*A_fb*(delta_fb+(tau-lamda)/2)^2);
V= (I_fb*(tau-lamda)^3)/((tau-lamda)^3 + 12*I_fb);
%%%%%%%%%%%%%%%%%%%%%
%%

% U=(A_fa*(tau-lamda)^3)/((tau-lamda)^3 + A_fa*(tau-lamda)^2 + 12*A_fa*(delta_fa+(tau-lamda)/2)^2);
% V= (I_fa*(tau-lamda)^3)/((tau-lamda)^3 + 12*I_fa);
gamma=asind( (12*(delta_fb+(tau-lamda)/2)/(tau-lamda)^3)*sqrt(U*V));
enforceLeft=(cosd(omega+gamma))/sind(omega);
enforceRight=sqrt(V/U)*(P*h/M);
enforceDiff=enforceRight-enforceLeft;
%% %%%%%%%%%%%%%%%%%%%%%%%%%%%%%%%%%%%%%%%%%%%%%%%%%%%%%
%%%%%%%%%%%%%%%%%%%%%%%%%%%%%%%%%%%%%%%%%%%%%%%%%%%%%
K1=((P/sqrt(2*U*h))*cosd(omega))+ (M/sqrt(2*V*h^3))*sind(omega+gamma);
K1_reduced= (P/sqrt(2*h*A_fb))*cosd(omega) + (M/sqrt(2*h^3*I_fb))*sind(omega);
omegaC=K1/(sigma*h^0.5);
K2=((P/sqrt(2*U*h))*sind(omega))+ (M/sqrt(2*V*h^3))*cosd(omega+gamma);
```

Vita

Sunday Aduloju was born to the late Mr. Victor Olorunshola, and Mrs. Wuraola Aduloju. He is the oldest of three brothers, Tope, Kayode, and himself, and younger sister Sola. In May 2015, he married his wife Sola, a nurse at National Hospital, Abuja. He has more than seven years' experience at National Engineering Design Development Institute, Nnewi. He earned his BS in Metallurgical and Materials Engineering from Federal University of Technology, Akure in 2006, and MS in Mechanical Engineering from Anambra State University in 2013. He began studying at the University of Tennessee in 2015 for Concurrent MS and PhD in Civil Engineering, obtaining his MS in Civil Engineering in 2018. He will continue the graduate program towards earning the PhD Degree.